Defence Research and Development Canada
Recherche et développement pour la défense Canada

DEFENCE R&D DÉFENSE

Numerical study of primary blast injury to human and sheep lung induced by simple and complex blast loadings

Amal Bouamoul
DRDC Valcartier

Defence R&D Canada – Valcartier
Technical Report
DRDC Valcartier TR 2008-245
December 2009

Canada

Report Documentation Page

Form Approved
OMB No. 0704-0188

1. REPORT DATE	2. REPORT TYPE	3. DATES COVERED
DEC 2009		**00-00-2009 to 00-00-2009**

4. TITLE AND SUBTITLE	5a. CONTRACT NUMBER
Numerical study of primary blast injury to human and sheep lung induced by simple and complex blast loadings	5b. GRANT NUMBER
	5c. PROGRAM ELEMENT NUMBER
6. AUTHOR(S)	5d. PROJECT NUMBER
	5e. TASK NUMBER
	5f. WORK UNIT NUMBER
7. PERFORMING ORGANIZATION NAME(S) AND ADDRESS(ES) **Defence R&D Canada - Valcartier,2459 de la Bravoure Road,Quebec, Quebec G3J 1X5 ,**	8. PERFORMING ORGANIZATION REPORT NUMBER
9. SPONSORING/MONITORING AGENCY NAME(S) AND ADDRESS(ES)	10. SPONSOR/MONITOR'S ACRONYM(S)
	11. SPONSOR/MONITOR'S REPORT NUMBER(S)

12. DISTRIBUTION/AVAILABILITY STATEMENT
Approved for public release; distribution unlimited

13. SUPPLEMENTARY NOTES

14. ABSTRACT

Detailed finite element models of two-dimensional horizontal slices of a human and a sheep thorax have been developed and validated with the limited data available in the open literature. The main goal of this study is to verify if the injuries observed in the animal are truly representative of human lung injuries for simple and complex blast loadings for different blast wave orientation. The sheep and human models were subjected to simple and complex blast loadings. In the case of simple blasts, nine curves that represent the threshold for lung injury and 1% and 50% probabilities of lethal lung damage for three different positive phase durations were simulated. Three different criteria were used for the assessment of lung damage from the numerical results. They are the maximum lung overpressure, the percentage of the lung volume as a function of the lung maximum pressure and the pressure-time history within the lung. Results showed that humans are predicted to have higher tolerance to blast than sheep. Lung damage development in sheep is predicted to be more dependent on the blast wave duration and orientation than in the human lung. In the case of complex blasts, three curves were simulated; each characterized by two different peak overpressures. Results show that damage to human and sheep lungs is considerable when the second peak overpressure closely follows the first one.

15. SUBJECT TERMS

16. SECURITY CLASSIFICATION OF:			17. LIMITATION OF ABSTRACT	18. NUMBER OF PAGES	19a. NAME OF RESPONSIBLE PERSON
a. REPORT	b. ABSTRACT	c. THIS PAGE			
unclassified	**unclassified**	**unclassified**	**Same as Report (SAR)**	**62**	

Numerical study of primary blast injury to human and sheep lung induced by simple and complex blast loadings

Amal Bouamoul
DRDC Valcartier

Defence R&D Canada – Valcartier

Technical Report
DRDC Valcartier TR 2008-245
December 2009

Principal Author

Dr. Amal Bouamoul

Defence scientist

Approved by

Dr. Dennis Nandlall

Section Head, Protection and Weapons Effects

Approved for release by

Christian Carrier

Chief Scientist

This study was done at DRDC Valcartier between February and December 2006, under the Numerical Modelling WBE of the 12RA Soldier Protection against Blast ARP.

Abstract

Detailed finite element models of two-dimensional horizontal slices of a human and a sheep thorax have been developed and validated with the limited data available in the open literature. The main goal of this study is to verify if the injuries observed in the animal are truly representative of human lung injuries for simple and complex blast loadings for different blast wave orientation.

The sheep and human models were subjected to simple and complex blast loadings. In the case of simple blasts, nine curves that represent the threshold for lung injury and 1% and 50% probabilities of lethal lung damage for three different positive phase durations were simulated. Three different criteria were used for the assessment of lung damage from the numerical results. They are the maximum lung overpressure, the percentage of the lung volume as a function of the lung maximum pressure and the pressure-time history within the lung. Results showed that humans are predicted to have higher tolerance to blast than sheep. Lung damage development in sheep is predicted to be more dependent on the blast wave duration and orientation than in the human lung. In the case of complex blasts, three curves were simulated; each characterized by two different peak overpressures. Results show that damage to human and sheep lungs is considerable when the second peak overpressure closely follows the first one.

Résumé

Deux modèles d'éléments finis d'une coupe horizontale du torse d'un humain et d'un mouton ont été développés et validés avec les quelques données disponibles en littérature ouverte. Les deux torses ont été soumis à des ondes de choc de types simple et complexe. Le but principal de cette étude est de vérifier si les dommages observés dans les poumons du mouton correspondent à ceux de l'humain.

Dans le cas d'ondes de choc simples, neuf courbes qui représentent le niveau de seuil, 1 % et 50 % de dommages aux poumons ont été simulées. Trois critères ont été utilisés pour évaluer les résultats numériques. Ce sont la pression maximale dans les poumons, le pourcentage du volume du poumon endommagé en fonction de la pression maximale du poumon et la pression dans les poumons en fonction du temps. Les résultats numériques ont montré que l'humain a une tolérance plus élevée à la surpression que le mouton et que les dommages dans les poumons du mouton dépendent plus de la durée et de l'orientation de l'onde de choc. Dans le cas d'ondes de choc complexes, trois courbes ont été simulées. Elles sont caractérisées par deux maxima de pression. Les résultats numériques ont montré que les dommages aux poumons des humains et des moutons sont considérables lorsque les premier et deuxième maxima de pression de l'onde complexe sont très rapprochés.

This page intentionally left blank.

Executive summary

Numerical study of primary blast injury to human and sheep lung induced by simple and complex blast loadings:

Bouamoul, A.; DRDC Valcartier TR 2008-245; Defence R&D Canada – Valcartier; December 2009.

The proliferation of blast weapons and the increased prevalence of large explosive charges (e.g. Improvised Explosive Devices) in current conflicts, may lead to an increase in the occurrence and severity of blast injuries especially those caused by blast overpressure (primary blast injuries). Within Defence Research & Development Canada, there is a need to understand and predict this type of injury in support of improved soldier protection.

Animal models are commonly used in published studies to establish the risk of lung injury from exposure to blast overpressure. However, there are concerns about the validity of animal models as a predictor for human injuries particularly in complex blast environments. Finite element models of human and sheep torsos have been developed and validated in order to verify whether the injuries observed in the animal are truly representative of human lung injuries for simple and complex blast loadings. A parametric study of the effect of torso orientation with respect to the blast wave direction was also performed. Results for the simple blast cases modelled showed that humans are predicted to have higher tolerance to blast than sheep and that the injuries to sheep lungs appear to be more dependent on the blast overpressure duration. In the case of complex blasts, modelled by multiple pressure peaks in the overpressure history, damage to the human and sheep lungs is considerable when the subsequent peak in overpressure is close to the first. An interesting result was noticed while studying the lung subjected to blast from different directions: human and sheep lung damage is strongly dependent on blast wave direction. Depending on the torso orientation, damage to the lung may range from severe to slight for a load level that is predicted to result in similar levels of injury according to Bowen primary blast injury curves.

The next step in this study will be to investigate different blast protection concepts in order to protect the human torso from blast overpressure. Concepts to be investigated include multi-layered material systems and varying the distance between the torso and the protective clothing.

Sommaire

Numerical study of primary blast injury to human and sheep lung induced by simple and complex blast loadings:

Bouamoul, A.; DRDC Valcartier TR 2008-245; R & D pour la défense Canada – Valcartier; décembre 2009.

La prolifération des armes à effet de souffle et la plus grande prédominance des grandes charges d'explosifs (par exemple, les engins explosifs improvisés) dans les conflits actuels peuvent entraîner une augmentation de l'occurrence et de la sévérité des dommages de souffle, particulièrement ceux provoqués par surpression de souffle (dommages primaires de souffle). Recherche et développement pour la défense Canada a un programme de recherche destiné à comprendre et prévoir ce type de dommage dans le but d'améliorer la protection du torse humain.

Un modèle d'éléments finis du torse d'un humain et d'un mouton a été développé et validé afin de vérifier si les dommages observés dans les poumons de l'animal correspondent à ceux de l'être humain pour des ondes de choc simples et complexes. Une étude paramétrique sur l'orientation du torse par rapport à la direction de l'onde de choc a été également réalisée. Les résultats numériques pour les ondes de choc simples ont démontré que les humains ont une tolérance plus élevée à l'effet de souffle que les moutons et que les blessures aux poumons des moutons dépendent de la durée de l'onde de choc. Dans le cas des ondes de choc complexes, les dommages aux poumons de l'humain et du mouton sont considérables quand les premier et deuxième maxima de pression de l'onde complexe sont très proches. Les dommages aux poumons de l'humain et du mouton dépendent de la direction de l'onde de choc. En effet, selon l'orientation de l'onde de choc par rapport au torse, les dommages aux poumons peuvent être légers ou graves.

La prochaine étape de cette étude est de proposer une nouvelle protection pour le torse contre l'effet de souffle. Cela sera fait en utilisant des matériaux multicouches et en variant la distance entre le torse et la protection.

Table of contents

List of figures

List of tables

This page intentionally left blank.

1 Introduction

Explosions have the potential to cause life-threatening injuries (e.g. blunt, penetrating wounds and blast overpressure injuries). The extent and pattern of injuries produced by an explosion are a direct result of several factors including the amount and composition of the explosive, the charge casing, the surrounding environment, the distance between the victim and the blast and any other environmental hazards. Blast injuries traditionally are divided into three major categories: primary, secondary and tertiary injuries. A person may be injured by more than one of these mechanisms in any given event. Primary blast injuries (PBI) are exclusively caused by the blast overpressure. Because air is compressible, a PBI usually affects air-containing organs such as the lung, ears and gastrointestinal (GI) tract. A secondary blast injury is caused by fragments that impact the body. A tertiary blast injury includes traumatic amputation and injuries sustained due to whole body displacement including impact (e.g. being thrown against another object) [Ref. 1].

The proliferation of blast weapons and the increased prevalence of large explosive charges (e.g. Improvised Explosive Devices) in current conflicts, may lead to an increase in the occurrence and severity of different blast injuries specially PBI. Within Defence Research & Development Canada (DRDC), there is a need to understand and predict this type of injury as well as the improvements to the torso protection.

In this optic, a numerical finite element (FE) model was built to predict blast injury from simple and complex blast overpressures [Ref. 2]. Using an advanced non-linear FE method, arbitrary Lagrangian-Eulerian formulation (ALE), two-dimensional models of the human and sheep thoraces were constructed. The main goal of this study was to find a correlation between the sheep and human, particularly as a function of orientation with respect to the blast wave and to verify if the injuries observed in the sheep are truly representative of human lung injuries. The next step of this study is to investigate different blast protection concepts in order to protect the human torso from blast overpressure. Concepts to be investigated include multi-layered material systems and varying the distance from the torso to the protective clothing.

2 Blast waves in air

2.1 Formation

Most conventional high explosives release, in a relatively short amount of time, a large quantity of energy through expansion of the gaseous detonation products. This results in an overpressure wave that travels through the air at a velocity greater than the speed of sound. As the blast wave propagates away from the centre of the explosion, its energy spreads through an increasing volume of air and the blast magnitude decreases rapidly. The passage of the blast wave through a particular position away from the detonation can be characterized as a simple or a complex blast wave. A simple blast-wave pressure disturbance resulting from an ideal explosion in free field has the shape of a Friedlander curve. Ideal explosions are defined as being produced by uncased bare charges, made with a conventional explosive (e.g. TNT, C4, RDX) with either a spherical or a hemispherical geometry. In the Friedlander curve, the pressure is comprised of a positive phase and a relatively long negative pressure phase as shown in Figure 1. Figure 1 shows also a comparison between an experimental blast wave and a Friedlander approximation.

This idealized variation in pressure versus time can be described by Equation 1 where P^+ is the peak pressure, T^+ is the positive phase duration, b is an empirically fit parameter and the time t is measured from the time of arrival, t_o. Complex blast waves can be described as any loading that does not fall under the description of a simple blast wave. Complex blasts may result from the reflection of a simple blast wave off the ground or other structures close to the explosive (e.g. in an enclosed space). Non-Friedlander blast waveforms can also be generated from non-ideal explosions. Non-ideal explosions include all explosions where the blast parameters deviate significantly from those produced by an ideal explosion. Examples of non-ideal explosions are cased munitions, IEDs and those where the blast wave is sustained by a prolonged combustion of the explosive.

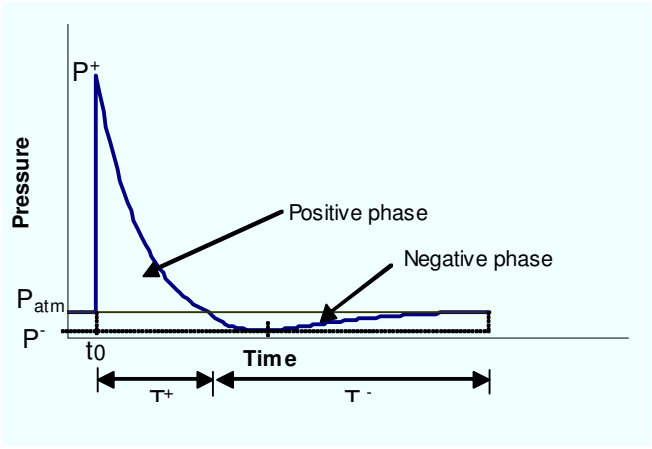

(a)

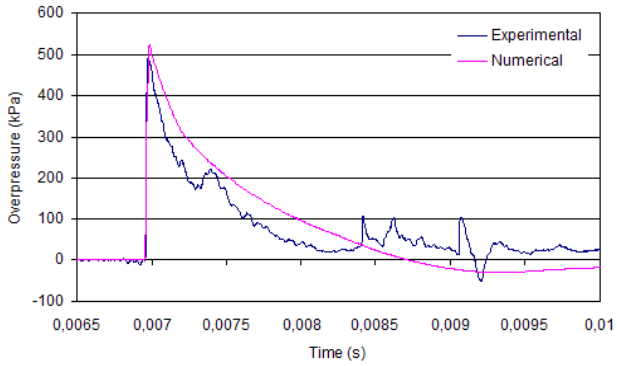

(b)

Figure 1: (a) Typical Friedlander pressure curve (simple blast), (b) comparison between a real blast wave and a Friedlander approximation (5 kg C4 at 2.5m).

$$p(t) = p_o + P^+\left(1-\frac{t}{T^+}\right)e^{\frac{-bt}{T^+}} \qquad (1)$$

2.2 Numerical blast implementation using ALE formulation

A hydrocode is a computational tool for modelling the behaviour of continuous media. It is used to solve problems where materials undergo large deformations over short periods. These codes can be based on either Lagrangian or Eulerian formulations.

The "classic" finite element (FE) method for structural mechanics is normally associated with the Lagrangian formulation in which the mesh follows the motion of the material. This method presents some difficulties when used to simulate non-linear and large deformation problems such as ballistic impact and high strain rate phenomena. These difficulties may include excessive mesh distortion as well as reduction in the time step needed to maintain stability in the solution. The second approach is the Eulerian formulation. In this approach, the computational grid is fixed in space while material passes through it. Among problems that are encountered when using Eulerian formulation to solve large deformation problems are the difficulty of simulating the interaction of multiple materials that may occupy one element.

To overcome such difficulties, a compromise between these two formulations is achieved by using an Arbitrary Lagrangian-Eulerian (ALE) formulation. In this approach, the mesh is free to move with the continuum in the normal Lagrangian way, or be held fixed in Eulerian manner, or, be moved in some way that is specified by the user (e.g. ascribe a velocity to the Eulerian mesh). The word “arbitrary” in “ALE formulation” refers to the fact that the combinations between Lagrangian and Eulerian methods are specified by the user through the selection of mesh motion to suit the requirements of the problem being modelled.

The short-term goal of this study is to develop a predictive model of human and sheep torsos with the ability to predict blast trauma for human and sheep lungs based on Bowen curves. The long-term goal of this research is to investigate different blast protection concepts in order to protect the human torso from blast overpressure. In order to achieve these two goals, an Arbitrary-Lagrangian-Eulerian (ALE) finite element formulation was chosen for the explosive and air elements. This was advantageous since the interaction among the blast flow, deformable body and future protection concepts may be significant.

2.3 Blast modelling in LS-DYNA

The LS-DYNA hydrocode is a general-purpose, hydrodynamic explicit FE code [Ref. 3]. It is used to analyze the non-linear dynamic response of two- or three-dimensional inelastic structures. Due to its explicit nature, the code uses small time steps to integrate the equations of motion and is especially efficient for solving transient dynamic problems. LS-DYNA was selected to simulate the coupled human/sheep torsos and blast waves.

Several methods for creating blast overpressure loading on solids in LS-DYNA were investigated. One method is modelling the detonation of an ideal explosive. This can be done with *MAT_HIGH_EXPLOSIVE_BURN model and an equation of state. However, this method is not useful since injuries from complex blast loadings have to be characterized. Another method is to use *LOAD_BLAST. This defines a free-field pressure-time history from conventional explosives (e.g. TNT, C4) and applies it directly to the surface of an object (fluid/structure interaction is not modelled). This method was not used since it was believed that possible coupling between the blast flow and the torso might be significant. Furthermore, this method does not model the flow around a bluff body, so the diffraction of the blast wave around the torso and any interaction this may have with the body would not be captured.

The other method is the ambient elements method. This method was chosen for its flexibility as it allows the desired overpressure and pulse duration to be generated using user defined pressure-time histories and a significant level of control over the waveform that results. To generate a blast wave, the FE domain representing the air around the torso is modelled as two regions: a high-pressure region at the inflow boundary for the blast overpressure wave and an ambient pressure region at 101.3 kPa in the remainder of the domain for air. Figure 2 shows an overview of the air and ambient mesh used in this study.

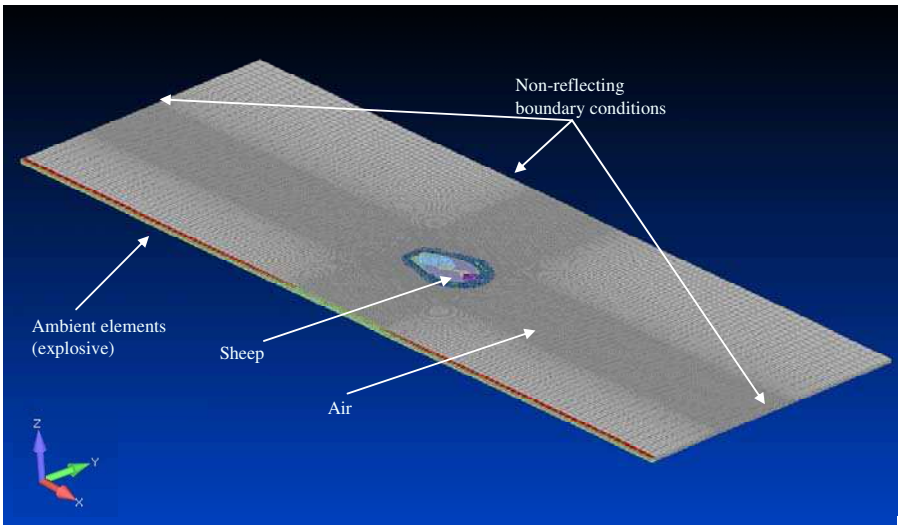

Figure 2: View of air and ambient elements.

Ambient elements act like a reservoir of high pressure and are given the desired blast profile. Because of the gradient pressure between ambient air (101.3 kPa) and ambient elements (high pressure), the pressure-wave moves toward the torso. A comparison

between a real blast test and the output generated with the ambient elements is given in Figures 1 and 33. The use of ambient elements requires material parameters as detailed in Table 1. Note that the density stays constant during calculation.

Table 1: Air parameters

Density, kg/m^3	1.293
Specific heat capacity at constant volume, J/kg-K	718
Specific heat capacity at constant pressure, J/kg-K	1005
Initial temperature, K	270

To use the ALE technique in LS-DYNA, solid elements are necessary. The human/sheep torso model, which has a Lagrangian mesh, has to be completely surrounded by air (Eulerian part). A thin layer of air and ambient elements, equal to 1.4 cm was used. This thickness corresponds to a representative slice of a torso taken between the fifth and sixth vertebrae level of an 82-kilogram man. Even though solid elements were used, the approach employed led essentially to a two-dimensional model by only using a thin layer of air and specific boundary conditions (see section 2.4).

The air and ambient domains were modelled with four layers of elements through their thicknesses. Air and ambient domains were meshed respectively using 8-node hexahedron elements with 104232 and 808 elements respectively. To allow a greater mesh density in the test area containing the thorax models, the air mesh was biased through the centre region (Figure 2). The coarse areas of the mesh correspond to a mesh spacing of 40 mm while the fine mesh is spaced at 5 mm. These variations in the air elements allowed better fluid/structure coupling while maintaining reasonable computation time. Finally, the air was modelled using the *MAT_NULL card and the ideal gas equation of state.

2.4 Displacement boundary conditions

Boundary conditions include fixed nodes along the (y-z) and (z-x) planes of the explosive and air boundaries. All nodes on the upper and lower (x-y) planes are fixed with respect to z-translation, x-rotation and y-rotation. In addition, non-reflecting boundary conditions were applied to the three free air edges to avoid the reflection of the blast wave at the edge of the Eulerian domain as shown in Figure 2.

2.5 Air – torso interaction

Along the torso wall boundaries, the air particle velocity is coupled to the torso mesh. The laws of kinematics require that no particles can cross the interface of the torso. Extra conditions were needed to ensure that the fluid and structural domains would not

detach or overlap during the simulation. These coupling conditions were achieved by applying a penalty coupling method using *CONSTRAINED_LAGRANGE_IN_SOLID as implemented in LS-DYNA.

To allow better coupling between the Lagrangian and the Eulerian parts, the default parameters in the *CONSTRAINED_LAGRANGE_IN_SOLID card were not used. If the density of the air or the torso mesh is too coarse in some blast wave situations, there can be a leakage through the fluid/structure interface. To void the fluid penetrating the torso mesh, the leakage parameter (ILEAK) was set equal to 2. This option, which uses a strong leakage control algorithm, may add energy to the system. This energy is eventually transformed into heat, which may cause a non-physical pressure rise. To avoid this problem, the equivalent amount of energy that was added to the system is removed from the kinetic energy. This technique is only available in the latest version of LS-DYNA (ls970) which is the one used in this study.

Another way to prevent the leakage is to increase the "Quadrature" parameter (NQUAD) from 0 to -4. NQUAD is the number of points (where virtual springs are used for contact purpose) assigned to each surface on the Lagrangian segments for coupling purpose. The negative sign means that the nodes at the end of each segment were also used in the coupling algorithm. Table 2 summarizes the *CONSTRAINED_LAGRANGE_IN_SOLID card parameters used for coupling purpose.

*Table 2: *CONSTRAINED_LAGRANGE_IN_SOLID parameters.*

SLAVE	MASTER	SSTYP	MSTYP	NQUAD	CTYPE	DIREC	MCOUP
				-4	4	3	0
START	END	PFAC	FRIC	FRCMIN	NORM		
0	1.0E10	0.2	0	0	0		
CQ	HMIN	HMAX	ILEAK	PLEAK			
0	0	0	2	0.2			

3 Blast injury

3.1 Primary, secondary and tertiary injuries

Blast injuries are inflicted on individuals subjected to a rapid rise in ambient pressure. The magnitude of damage due the blast wave is dependent on:

- the peak of the initial positive pressure wave;
- the duration of the overpressure; and
- the degree of focusing and reflection due to a confined area or walls.

Commonly, blast injuries are divided into three main classes: primary, secondary and tertiary, as well as two further classes that cover burns and toxicity. In general, primary blast injuries are characterized by the absence of external injuries. Internal injuries resulting from PBI are frequently unrecognized and their severity underestimated. The inertia and pressure differentials are the main mechanisms involved in the pathogenesis of PBI. Therefore, the majority of prior research focused on the mechanisms of blast injuries within gas-containing organs such as the auditory system, respiratory system and gastrointestinal tract. Lung hemorrhage which is the area of interest in this study causes a lack of oxygen in all vital organs specially, the brain which may lead to a coma.

Secondary injuries are due to the impact of debris and fragments and are the most common. These injuries may affect any part of the body and sometimes result in visible haemorrhage.

Tertiary injuries include amputation and any injuries sustained due to whole body displacement and being thrown against other objects. These injuries are generally characterised by blunt trauma, including bone fractures.

3.2 Bowen curves

The Bowen curves were created after analyzing a wealth of data, primarily from shock tube testing of two groups of animals: small animals, such as mice, pigs and rabbits and large animals, such as monkeys, sheep and swine. The Bowen curves are a relevant method to estimate primary injuries from a simple (Friedlander) blast loading [Ref. 4]. Using the blast wave duration and the peak overpressure one can estimate the probability of the survivability of a human when exposed to a Friedlander type overpressure wave. Due to a limited amount of data on human tolerance to blast, the curves generated from the experimental results from the large animal group were scaled to approximate a 70-kilogram man. Figure 3 shows the Bowen curves for a man oriented perpendicular to the blast direction. In this figure, three versions of curves are given: The original curves [Ref. 4], a set of curves revised by Richmond [Ref. 5] and a new set of survivability curves by Bass et al. [Ref. 6] based on a complete reanalysis of

the original data supplemented by additional data from more recent sources. When this study was performed, only the original and revised curves were available, with the latter presumed to represent the current state of the-art. Consequently, the results of this study were based on the revised Bowen curves by Richmond. There are plans to reassess the model predictions in view of the new curves published by Bass *et al.*

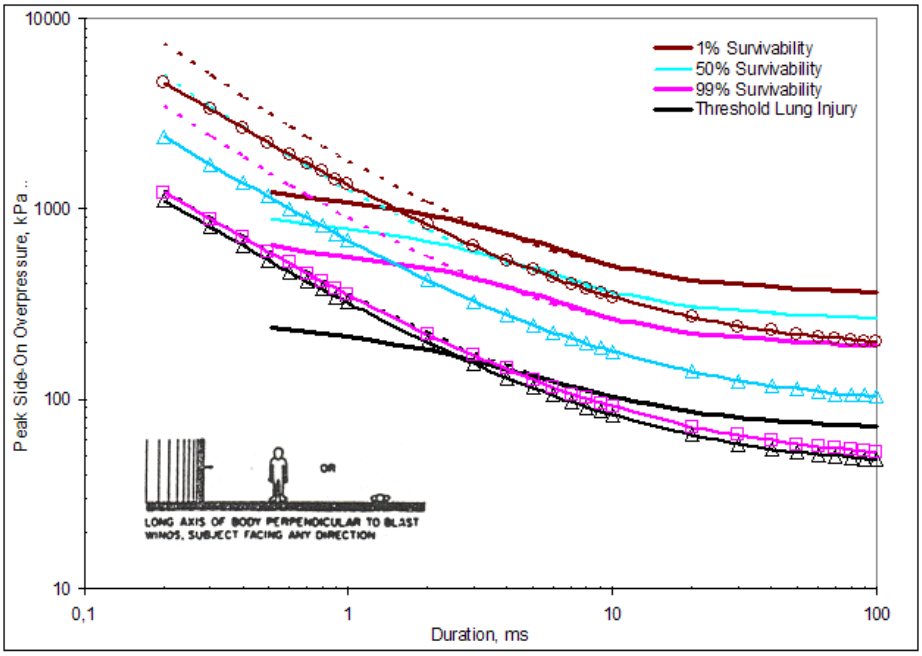

Figure 3: Original, revised version and new Bowen curves for a man oriented perpendicular to the blast direction, (dashed lines: original curves [Ref. 4], stretch lines: revised curves [Ref. 5], dashed lines with symbols: new curves [Ref. 6])

In Figure 3, the original and revised Bowen curves are identical when the blast wave duration is longer than 2 ms. When the blast wave duration is shorter than 2 ms, the original and revised Bowen curves diverge. In fact, for the same short duration (0.5 ms), using the original Bowen curve, the peak overpressure that induces 1% lethality is equal to 1560 kPa compared to only 640 kPa for the revised curves, a significant difference. The original curves were based on two data sets, one for short duration blasts and another for longer durations. In his revision of the original data, Richmond was addressing concerns over some the data treatment used to calculate the peak pressures for the shorter duration data set. The reanalysis of the data led Richmond to conclude that the peak pressures applied to the curves were too high. As a result, the shorter duration end of the curves shifted down indicating a lower tolerance to short duration overpressures than was predicted by the original curves.

Ambient elements were used to ascribe specific thermodynamic states to boundary elements in the fluid mesh, which represent the incident overpressure history generated by a given blast and standoff. The temperature histories applied to the ambient elements in the numerical simulations correspond to a specific peak pressure and duration. The level of injury depends on the blast wave characteristics, which are the positive phase duration and the incident peak overpressure. Nine Friedlander (simple blast) curves representing the threshold level (TH), 1% and 50% of lung damage (LD_1 and LD_{50}) for durations equal to 0.4 ms, 2 ms and 5 ms on the revised Bowen curves were selected. These curves and their characteristic peak pressures and durations are listed in Table 3. An abbreviation for these curves is used throughout the report. For example, TH-T_{04}-P_{250} refers to a threshold blast wave with duration equal to 0.4 ms and a peak overpressure of 250 kPa. Similarity, LD_1-T_2-P_{500} refers to an LD_1 blast wave with duration equal to 2 ms and a peak overpressure of 500 kPa.

Table 3: Characteristics of the blast waves using during the simulations

	TH	TH	TH	LD_1	LD_1	LD_1	LD_{50}	LD_{50}	LD_{50}
Peak overpressure, kPa	250	200	130	640	500	350	890	700	500
Positive phase duration, ms	0.4	2	5	0.5	2	5	0.5	2	5

The Bowen curves are still a relevant method to estimate the probability of lethality from a simple blast loading. They were used in this study as a baseline to validate the lung injuries criteria. In fact, trauma evaluation for the numerical model was determined within the lung. From the work done by O'Brien *et al* and Cooper *et al* [Refs. 7, 8], pressure within the lung, exposure time and the rise time of the pressure are known to be associated with lung trauma. Experimental tests involving measurements of the intra-thoracic peak pressure have suggested a threshold between 70 kPa and 110 kPa for humans [Ref. 9]. The University of Waterloo has established a relation between intra-thoracic pressure and lung injury [Ref. 2] and suggested a relation between human lung injuries and lung overpressure, as shown in Table 4. Lacking any direction from the open literature on similar sheep-lung injury thresholds, the relation in Table 4 was also used to quantify the sheep lung injuries in this study.

Table 4: Lung pressure and associated injury and colour [Ref. 2].

	Severe	240 kPa and +
	Moderate	140-240 kPa
	Slight	100-140 kPa
	Trace	60-100 kPa
	None	60 kPa and -

4 Lagrangian parts

The human and sheep models described in this section were initially generated by Waterloo University under contract number W7701-024463/001/QCA [Ref. 2] based on the work done by O'Brien *et al* and Cooper *et al* [Refs. 7, 8].

4.1 Human model

Figure 4 shows a top view of the numerical and CT-scanned human torso components. The model was created by the University of Waterloo using pictures from the Visible Human Project, National Library of Medicine [Ref. 10]. The picture is for an 82-kilogram, 1.8 metre tall man and was taken at the fifth and sixth thoracic vertebrae level. The human model was modelled with four layers of elements through its thickness to approximate a 1.4 cm section of the mid-thorax (Figure 4).

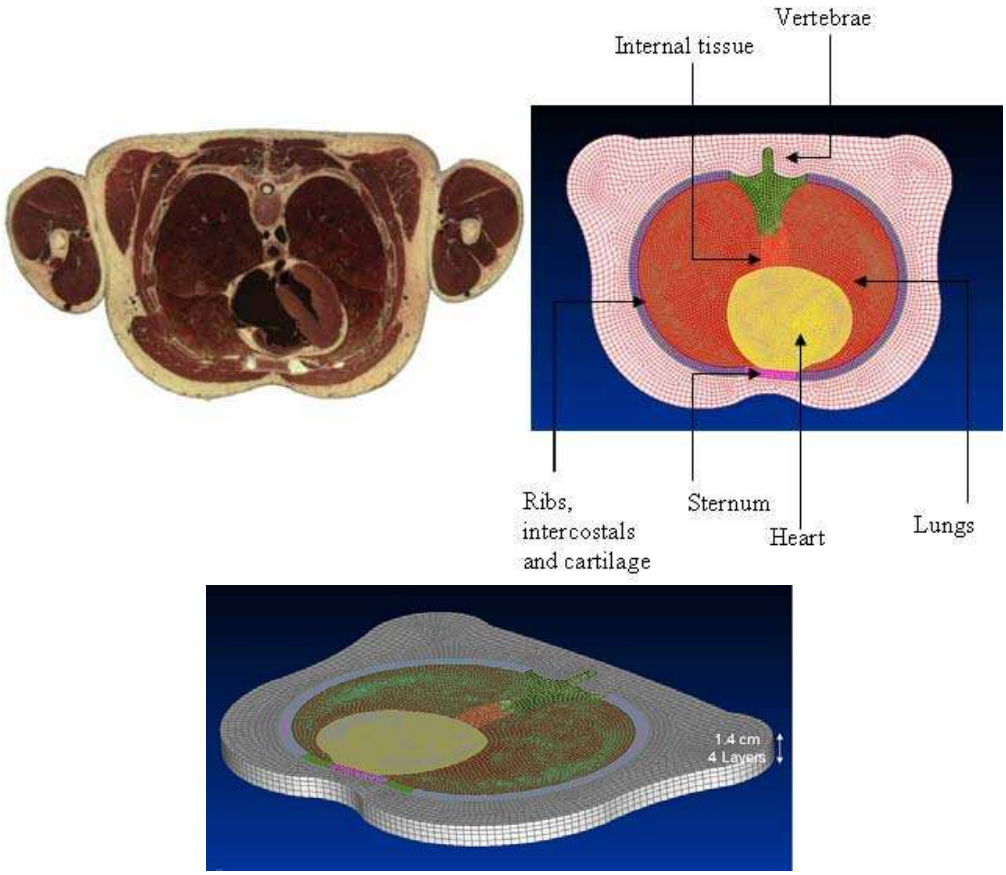

Figure 4: A top view of the numerical and actual human torso components.

The human section measures approximately 34.5-cm width and 23.2-cm depth. The human model consists of 34328 8-node hexahedron elements and 42165 nodes. The size of the human elements varies from 2.5 mm to 5 mm.

4.2 Sheep model

Figure 5 shows a top view of the numerical and CT-scanned sheep torso components. The sheep model was created using pictures from an atlas of x-ray anatomy of the sheep [Ref. 11]. The x-ray pictures were for a two-year old 56.6-kilogram ewe. They were taken at the fifth and sixth thoracic vertebrae level. The model was comprised of four layers of thickness elements to approximate a 1.4 cm section of the mid-thorax. The sheep section measures 26.1-cm width and 34.3-cm depth. The sheep model consists of 29857 8-node hexahedron elements and 36740 nodes. In order to maintain the ALE coupling, the sizes of the sheep elements were kept equal to or smaller than the size of the air elements surrounding the torso. The size of the sheep elements varies from 2.5 mm to 5 mm.

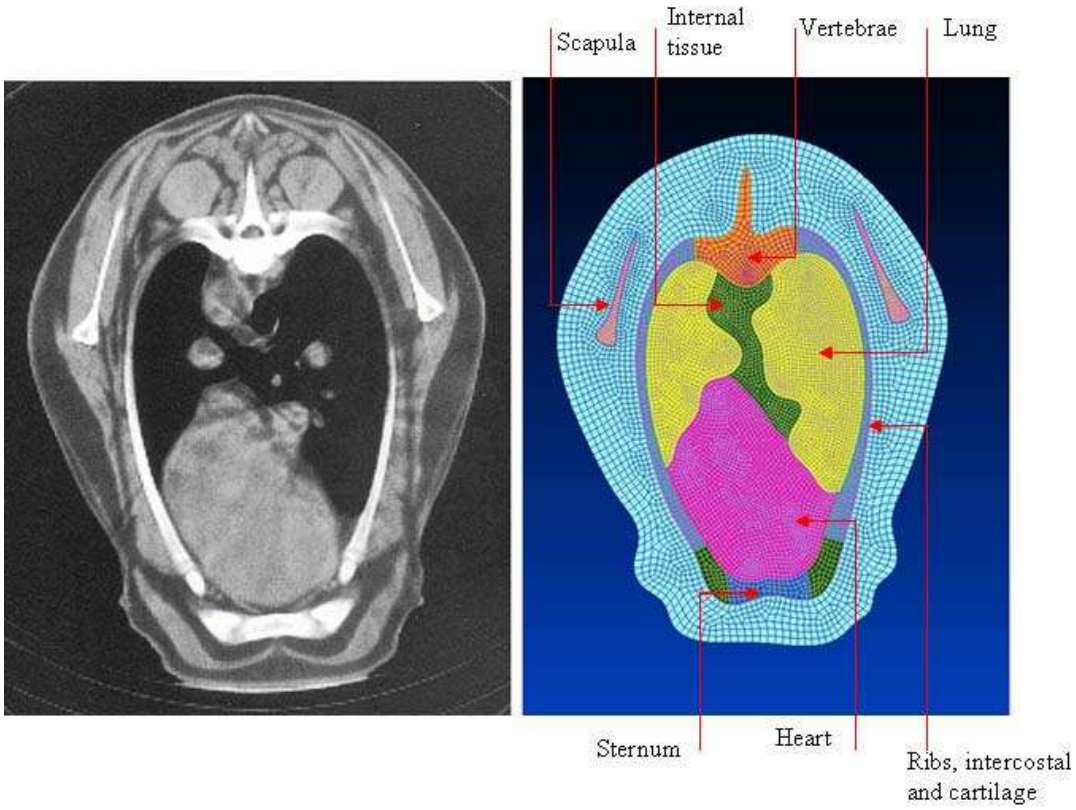

Figure 5: A top view of the numerical and actual human torso components.

4.3 Representation of rib cage

Because of the three-dimensional nature of the rib cage, the model was divided into two components: a bone level where the rib cage is represented by bone and an intercostal level where the structure of the rib cage is captured by modelling the intercostal muscle tissue. The different characteristics of bone (ribs) and muscle have an influence on wave propagation and hence on the injury that develops behind the rib cage. As a result, both structures were included in the model. The human and sheep rib cage models are shown in Figure 6 where the various components are labelled. The human and sheep torso models were oriented to the blast direction as shown in Figure 7.

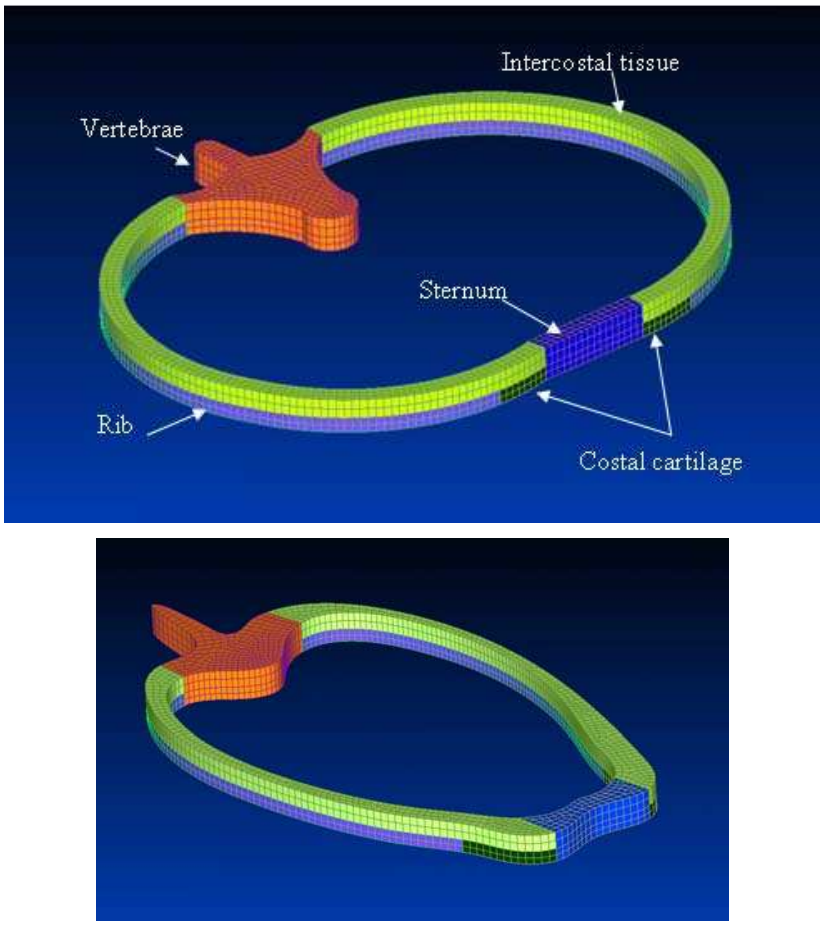

Figure 6: The FE human and sheep rib cages.

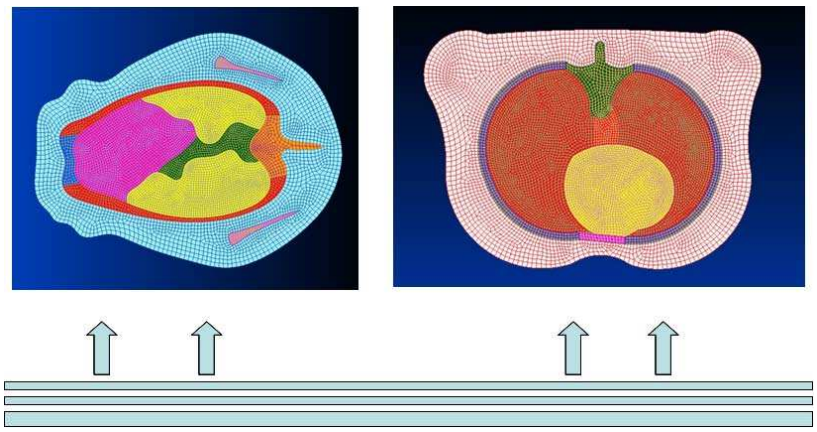

Figure 7: Blast wave direction.

4.4 Material properties

An extensive literature review focused on human and animal tissue material properties was performed by the University of Waterloo [Ref. 2]. Table 5 lists the material models used for the components of the sheep and human torso models as well as their principal mechanical properties. The MAT_SIMPLIFIED_RUBBER model, which consists of a set of piecewise linear stress-strain curves at discrete strain rates, was used to model muscle tissue, the heart, inner tissues and the intercostals. Ribs, the costal cartilage, the vertebrae and the sternum were modelled using the MAT_ELASTIC model. This model allows an isotropic elastic behaviour to be modelled without fracture or plastic strain. The MAT_ELASTIC model defines a linear relationship between the stress and the strain through the Young modulus. MAT_NULL model was used for the lung tissue. This model does not account for deviatoric stresses caused by changes of shape; however, the Gruneisen equation of state was used to predict the pressures that result from volumetric strain (hydrostatic stresses).

Using the velocity of a shock wave relative to the particle velocity curve (V_s-V_p), the Gruneisen equation of state calculates pressure based on volume change. The input required includes the speed of sound in the uncompressed material and the slope of the (V_s-V_p) curve described by S_1, S_2 and S_3 parameters which are equal to 1.92, 0 and 0 respectively [Ref. 3].

Table 5: Material properties for each part of the human and sheep torsos

	MATERIAL MODELS	**DENSITY** (kg/m^3)	**YOUNG MODULUS** (Pa)	**POISSON RATIO**	**BULK MODULUS** (Pa)
Tissue (muscle)	MAT_SIMPLIFIED _RUBBER	1050	N/R	N/R	2.2×10^9
Heart					
Inner tissue					
Intercostals					
Ribs	MAT_ELASTIC	1561	7.9×10^9	0.379	10.9×10^9
Lung	MAT_NULL	200	N/R	N/R	N/R
Vertebrae	MAT_ELASTIC	1644	9.6×10^9	0.376	12.9×10^9
Costal cartilage	MAT_ELASTIC	1281	49×10^6	0.4	81.6×10^6
Sternum	MAT_ELASTIC	1354	3.5×10^9	0.387	5.2×10^9

N/R: Not Required

5 Assessment of the numerical model

The simulations were run for a period of 0.01 s after which, pressure was plotted for all elements in the human and sheep lung. Three different injury criteria were used for the assessment of the numerical results: the maximum lung overpressure, the percentage of the lung volume as a function of the lung maximum pressure and the pressure-time history within the lung. The combined analysis of numerous simulations from the current study and the University of Waterloo research [Ref. 2] have shown that lung tissue close to the rib cage at the intercostal level, where the rib cage is represented by intercostal muscle tissue in both FE models, has high pressure (more injury) when subject to blast overpressure than the lung tissue in the bone level where the rib cage is represented by bone. This high pressure comes from the fact that the rib cage does not shield the lungs. Further into the lung, this effect is mitigated as the waves diffract around the ribs. As a result, the evaluation of the numerical model in this report was based on the elements located in the intercostal level of the human and sheep FE models.

5.1 Maximum lung overpressure

In terms of predicted pressure, the lung generally showed the highest pressures, consequently, the highest possibility of injury. In both cases, human and sheep lung, high pressures that exceed the threshold (70 kPa) are generally located in the torso side facing the blast (see Figure 7). Figure 8 compares the maximum lung overpressure in the sheep and the human torsos and lungs.

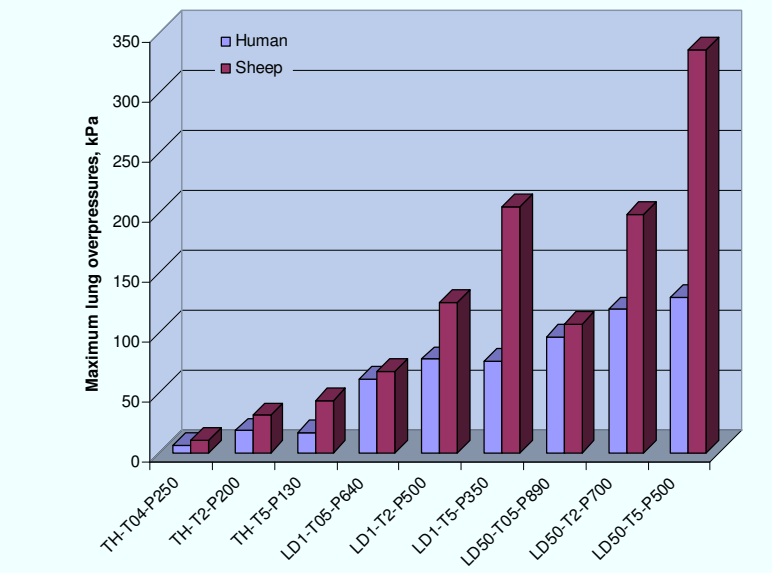

Figure 8: Maximum human and sheep lung overpressure.

Based on the threshold peak pressure for lung tissue damage, which is assumed to be 70 kPa (see section 3.2), the numerical model predicts the transition from no injury (TH) to injury (LD). In fact, the maximum lung overpressure for the three threshold cases (TH-T_{04}-P_{250}, TH-T_2-P_{200} and TH-T_5-P_{130}) does not exceed 70 kPa. This is also seen in Table 6 where the lungs are practically blue in colour (low pressure). It is worth mentioning that the high pressure (red colour) on the lower part of lungs in the three threshold cases comes principally from the shape and the size of the elements in this region of the lungs. Element size in this region is small compared to other elements in the lungs and has a non-square shape. This would lead to the elements being distorted, which leads to high non-physical pressure.

Numerical results show that humans have a higher tolerance to blast, which is in general accordance with the Bowen study stating that the large animal group including sheep have lower tolerance to blast than primates do.

Even though the human model predicts a relatively constant value of maximum overpressure for all injury levels, the sheep model appears to be more dependent on the blast duration. The lung material properties, geometry and the orientation of the two specimens could explain the difference between the sheep and human response. Since the two torsos are modelled with the same material properties, the geometry of the sheep and its orientation are likely the most important factors to consider.

Within the same injury level (e.g. TH, LD_1 and LD_{50}), the peak lung pressure increases as the duration of the incident blast pressure increases. This is somewhat dissimilar to the Bowen curves, which indicate that the loading cases selected should result in comparable levels of injury (i.e. the three peak-pressure durations selected are on iso-injury curves).

Tables 6 and 7 summarize the predicted blast injury pattern in the lung from the nine different Friedlander blast waves for the human and sheep models respectively. The distribution of peak pressures in the FE lung ranged from no injury, trace, slight, moderate to severe based on the threshold peak pressures discussed above in section 3.2. Damage to the human lung is more significant at the intercostal level and around the edges of the lung. The former is believed to be related to a shielding effect of the ribs as it is local to the area immediately behind the rib cage. The latter can be explained by the reflecting wave from the heart, vertebrae and ribs where the densities are higher than the lung density. In the case of the sheep lung, damage to the lung is severe in the larger lung (the right lung) since it is the one exposed to the blast. Figure 9 shows a typical progression of the pressure wave as a function of time. The pressure contours were plotted at times: 0, 0.9 ms, 1.8 ms, 3.6 ms, 5.4 ms and 7.2 ms.

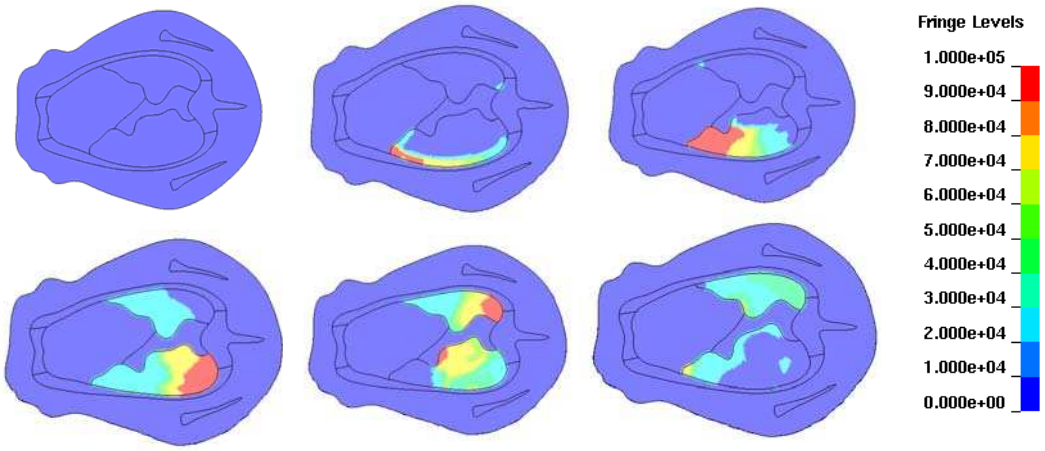

Figure 9: Wave propagation in the sheep torso at different time steps.

Table 6: Blast damage from different blast waves, human model

	T = 0.5 ms	***T = 2 ms***	***T = 5 ms***
LD_{50}	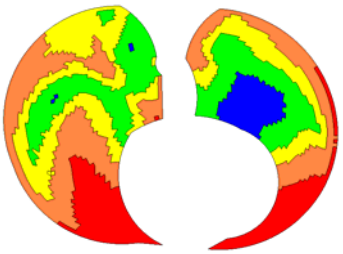	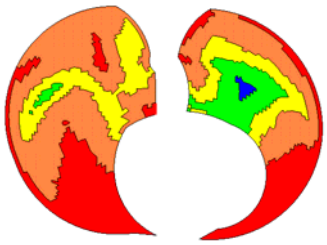	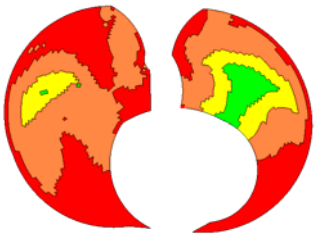
LD_1	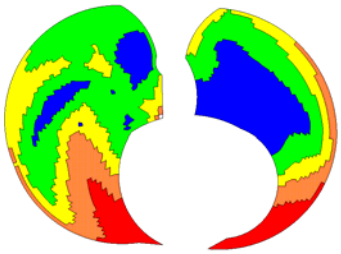	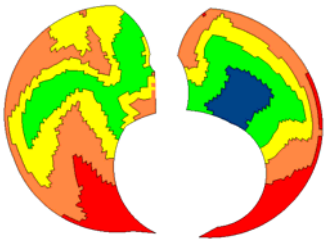	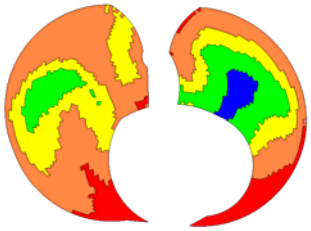
TH	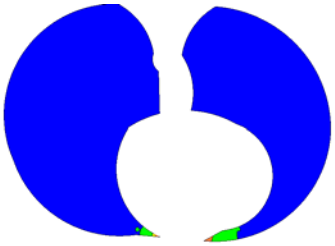	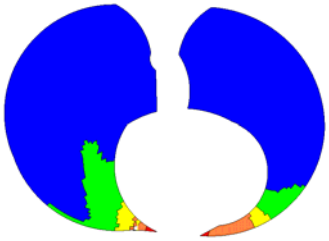	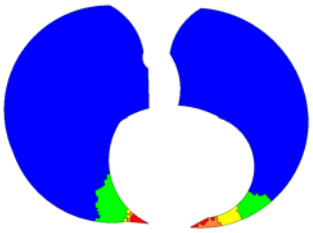
	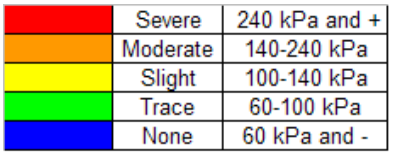		

Table 7: Blast damage from different blast waves, sheep model

	T = 0.5 ms	***T = 2 ms***	***T = 5 ms***
LD_{50}	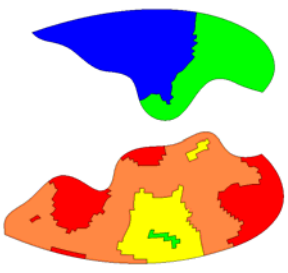	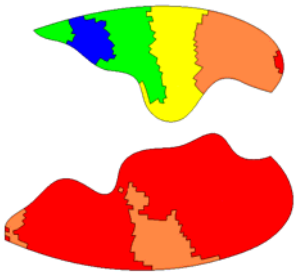	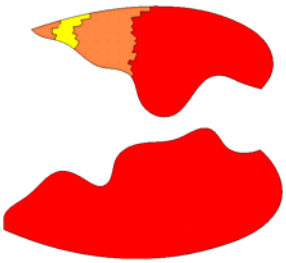
LD_1	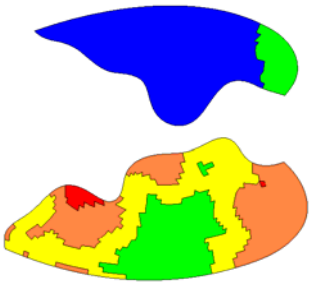	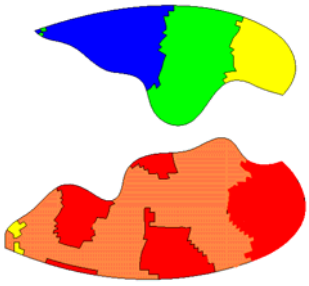	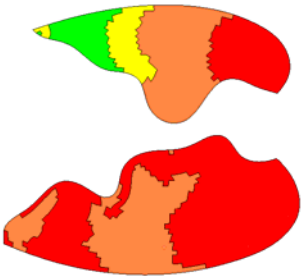
TH	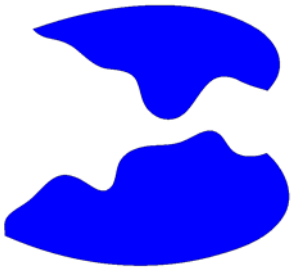	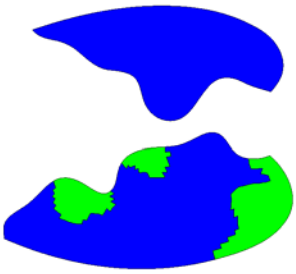	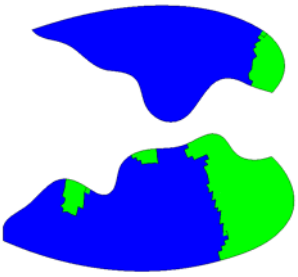
	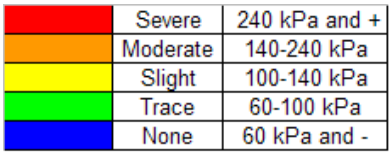		

	Severe	240 kPa and +
	Moderate	140-240 kPa
	Slight	100-140 kPa
	Trace	60-100 kPa
	None	60 kPa and -

5.2 Percentage of lung volume as a function of lung maximum pressure

Figures 10 and 11 show the percentage of lung volume reaching a given maximum pressure. As one might expect from the impulse transmitted to the thorax for these cases, the graph is bounded by the TH-T_{04}-P_{250} and LD_{50}-T_5-P_{500} results. In Figure 10, the LD_1-T_5-P_{350} case is more severe than the LD_{50}-T_{05}-P_{890} in the human torso model. Based on the assumption that peak pressure is related to damage in the tissue, it was predicted that a greater percentage of tissue would be damaged. Results for the sheep model (Figure 11), the LD_1-T_5-P_{350} and LD_1-T_2-P_{500} cases are more severe than the LD_{50}-T_5-P_{500} and LD_{50}-T_{05}-P_{890}, which is in contradiction to the Bowen curves. Also, the LD_{50}-T_{05}-P_{890} and LD_1-T_2-P_{500} appear to have the same injury profile in terms of the percentage of human lung volume injured.

The model also predicts that damage to the lung is more significant for long duration overpressure histories than it is for short duration blast overpressures in both human and sheep torsos. For example, in the human LD_{50}-T_{05}-P_{890} and LD_{50}-T_5-P_{500} cases, the maximum lung pressure exceeded 240 kPa in 16% and 41% of the lung volume respectively. For the sheep, these values were 21% and 93% for the LD_{50}-T_{05}-P_{890} and LD_{50}-T_5-P_{500} cases. These results can be linked to the total impulse of the incident pressure wave. Assuming the Freidlander pressure profile, the total impulses for the LD_{50}-T_{05}-P_{890} and LD_{50}-T_5-P_{500} cases are approximately 130 Pa-s and 1030 Pa-s.

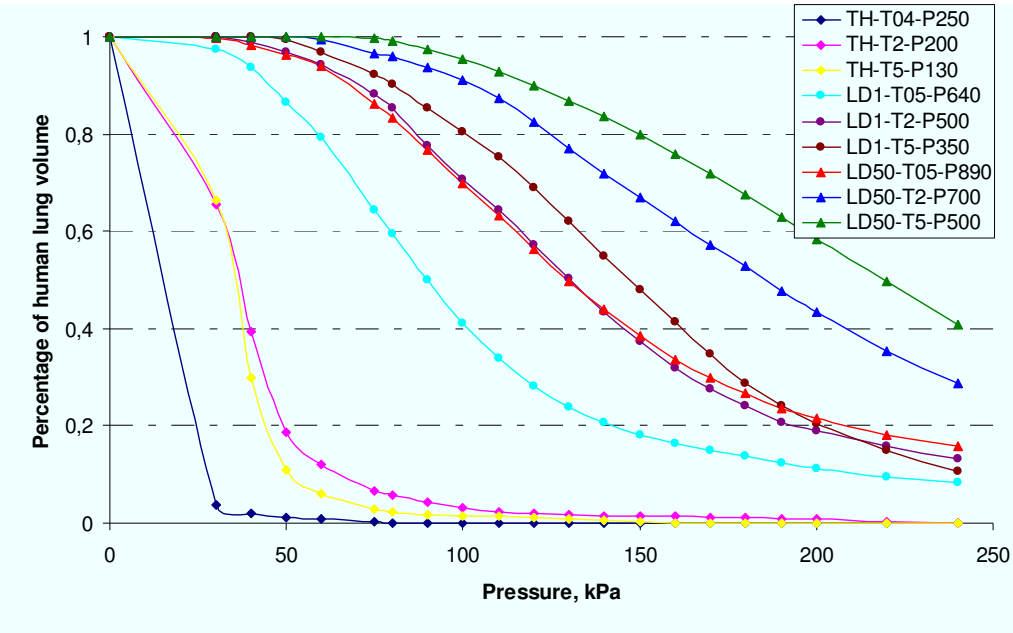

Figure 10: Percentage of human lung volume.

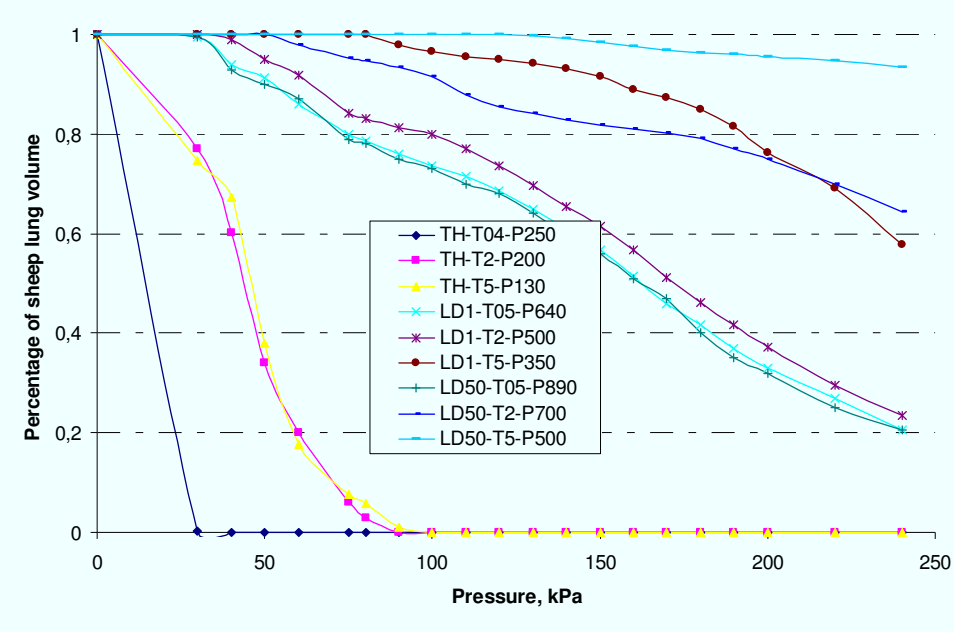

Figure 11: Percentage of sheep lung volume.

5.3 Pressure-time history

The lungs in the human and sheep models were "instrumented" with numerical gauges to record the element pressure histories at different locations. Three pressures histories were gathered from each numerical model at the locations illustrated in Figure 12. The elements are located in the first intercostal layer of the model. Figures 13 to 20 show the pressure-time history of representative sheep and human elements for the TH, LD_1 and LD_{50} levels.

From these curves, an interesting trend was noticed in the lungs subject to short and long duration incident blast overpressures for the same nominal level of injury according to the Bowen curves. It was seen that the long duration blasts (5 ms) induce higher pressure in the sheep lung than in the human lung in all injury cases. In all 5 ms blast-overpressure duration cases, pressure in the sheep lung is approximately twice that predicted in the human lung. Since the sheep and human lung were modelled with the same material properties, this would indicate a significant geometric effect that would suggest a higher tolerance to blast in humans. This observation is in accordance with the Bowen study, which suggested that primates might have a higher tolerance than the large animal group used in the experiments, including sheep.

Short-duration blast overpressure histories (0.5 ms) produced higher pressures in the front of the lung than in the rear in both the human and sheep models, which is reasonable and expected. However, long-duration blasts (5 ms) caused more damage at the rear of the human and sheep lungs. These tendencies are in agreement with the Bowen research, which states that long duration blasts result in injuries on the opposite side of the animal while short duration blasts generated more significant injuries on the lung surface facing the blast.

In all results from the sheep model, the left gauge element starts monitoring a pressure rise before the right gauge element (see Figure 12). This is due to the scapula, which initially acts as a barrier to the blast wave and shields the right gauge. When the blast hits the sheep, the blast wave arrives at the left gauge first and then propagates throughout the lung. However, the pressure recorded by the right gauge is generally higher than that recorded by the left gauge. This may be due to the reflection from the scapula (high material density) that leads to an increase in the intensity of the pressure.

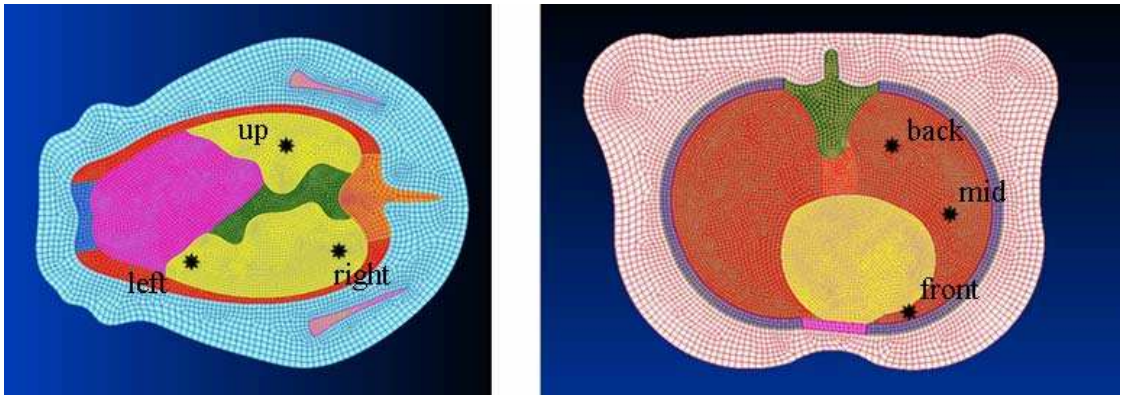

Figure 12: Gauge locations, left (sheep) and right (human)

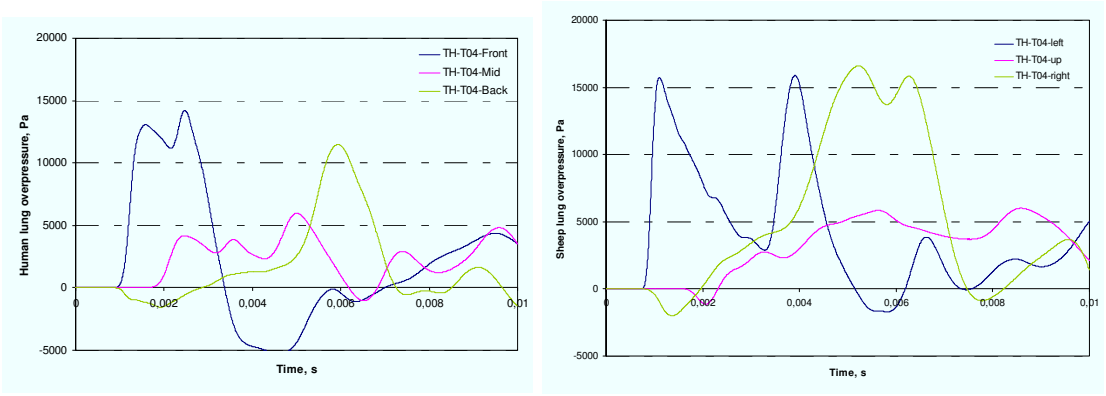

Figure 13: Human (left) and sheep (right) lung overpressure, TH-T_{04}-P_{250} case.

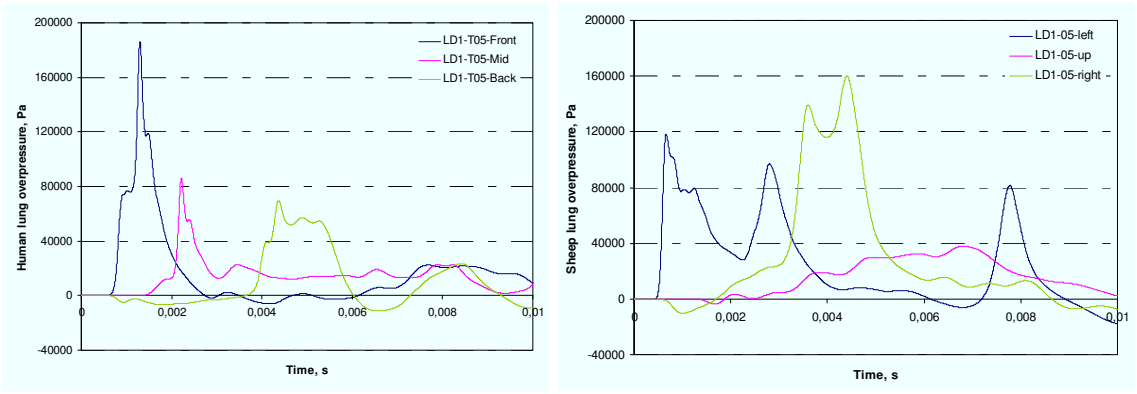

Figure 14: Human (left) and sheep (right) lung overpressure, LD_1-T_{05}-P_{640} case.

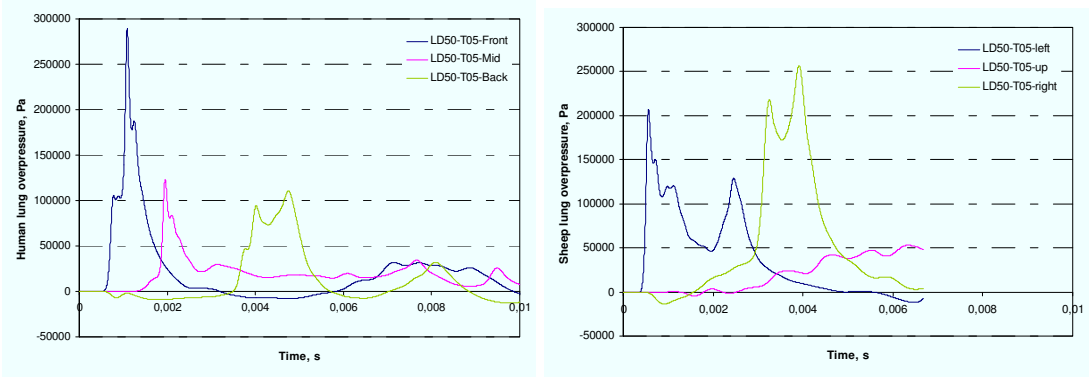

Figure 15: Human (left) and sheep (right) lung overpressure, LD_{50}-T_{05}-P_{890} case.

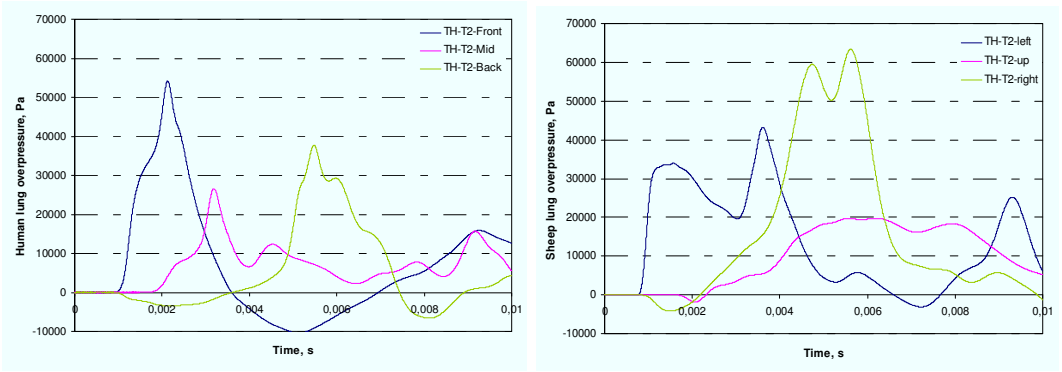

Figure 16: Human (left) and sheep (right) lung overpressure, TH-T_2-P_{200} case.

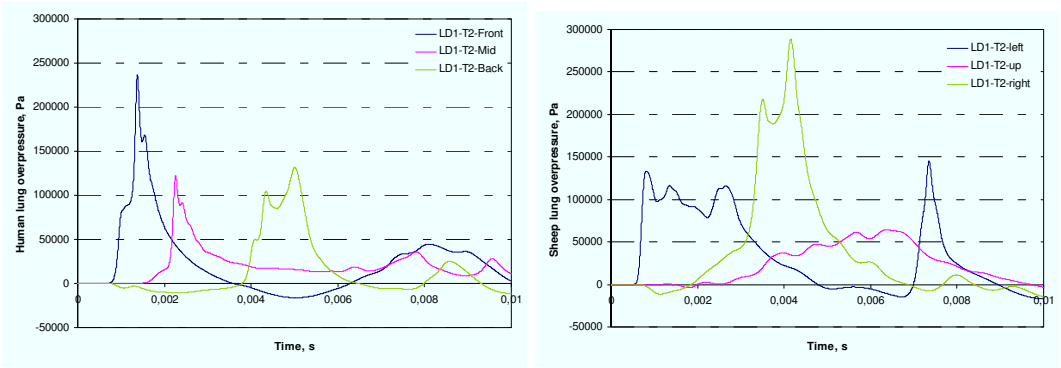

Figure 17: Human (left) and sheep (right) lung overpressure, LD_1-T_2-P_{500} case.

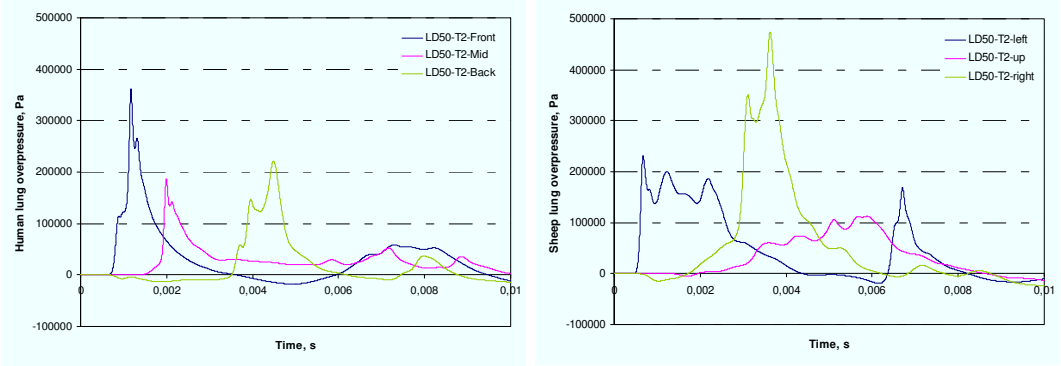

Figure 18: Human (left) and sheep (right) lung overpressure, LD_{50}-T_2-P_{700} case.

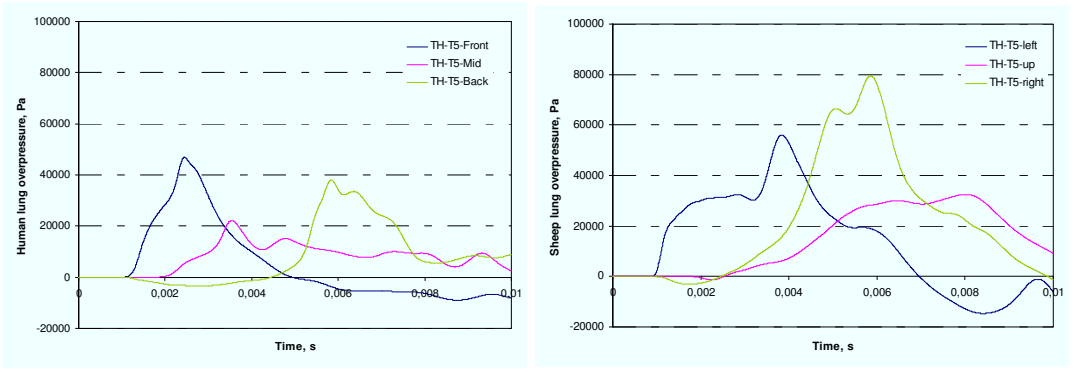

Figure 19: Human (left) and sheep (right) lung overpressure, TH-T_5-P_{130} case.

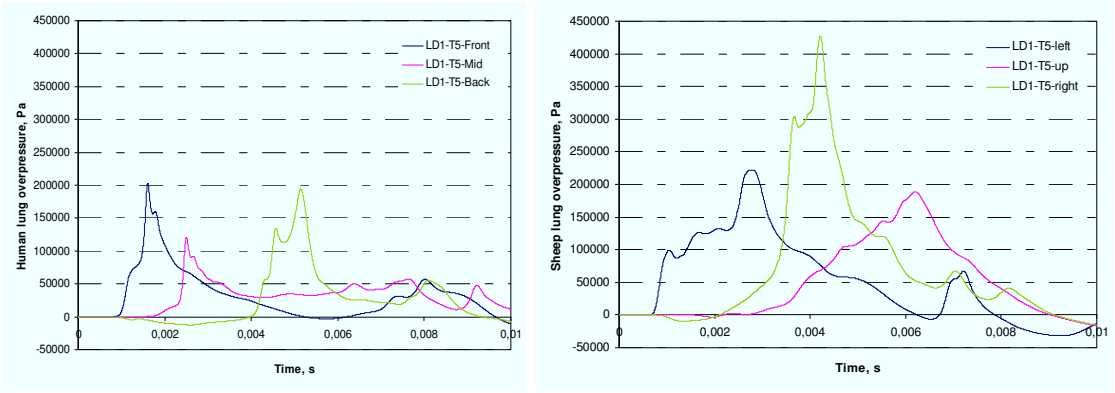

Figure 20: Human (left) and sheep (right) lung overpressure, LD_1-T_5-P_{350} case.

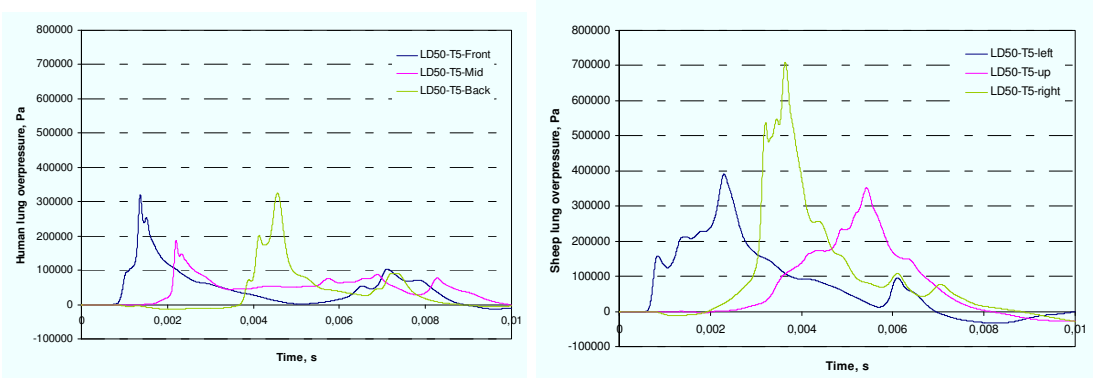

Figure 21: Human (left) and sheep (right) lung overpressure, LD_{50}-T_5-P_{500} case.

6 Effect of body orientation on the blast injury

The intensity and type of trauma inflicted on a body by a blast overpressure are related to many factors. Among these factors is body orientation. In order to study this factor, the sheep and human models were exposed to blast waves from different sides. In total, twelve orientations were simulated at three different blast injury levels that correspond to the 2 ms duration (TH-T_2-P_{200}, LD_1-T_2-P_{500} and LD_{50}-T_2-P_{700}). The sheep and the human torsos were rotated around their vertical axes in 30 degree increments starting from 0 to 330 degrees. Two types of results were examined from the simulations. The first were fringe plots of maximum peak overpressure from the elements in the intercostal layers of the models. The second were the average of the maximum overpressure readings of twelve elements located in the human torso and lung model and six elements located in the sheep lung model, as shown in Figures 22 and 23 respectively. These pressures were averaged from virtual gauges in both the intercostal and rib layers of the mesh.

Polar plots of the average maximum overpressure give a qualitative assessment of the effect of the blast orientation on the human and sheep torso injuries. In the human model, the average of the G1 to G4 virtual gauge maximum overpressures is referred to as the *back* curve. The curve labelled *mid* corresponds to the average of the G5 to G8 virtual gauge maximum overpressures and the curve labelled *front* is the average of the G9 to G12 virtual gauge maximum overpressures. All the human gauge data is presented in Annex A. In the sheep case, the curve labelled *left* represents the average of virtual gauges G1 and G2 maximum overpressures. The curve labelled *right* is the average of G3 and G4 gauges maximum overpressure data and the curve labelled *up* corresponds to the average of the G5 and G6 virtual gauge maximum overpressures. 0 degree orientation was used in the sections described so far.

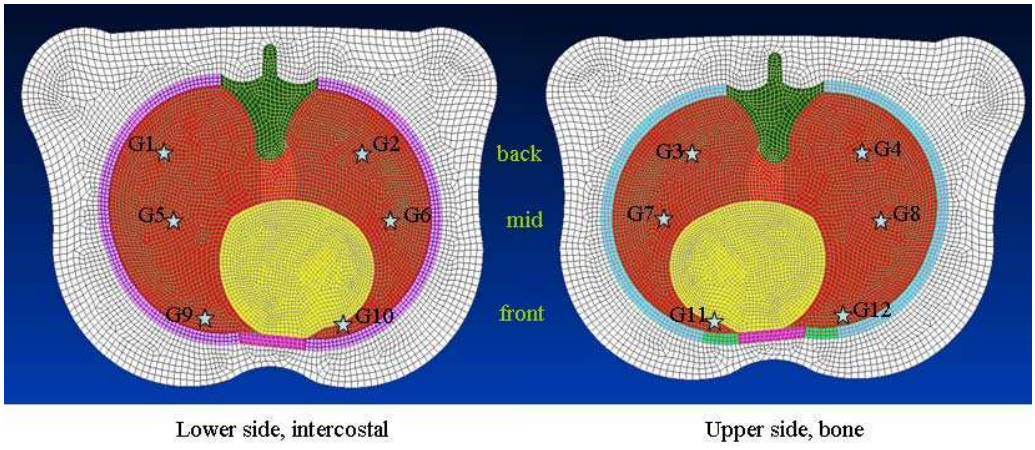

Figure 22: Gauge locations for body orientation inputs, human

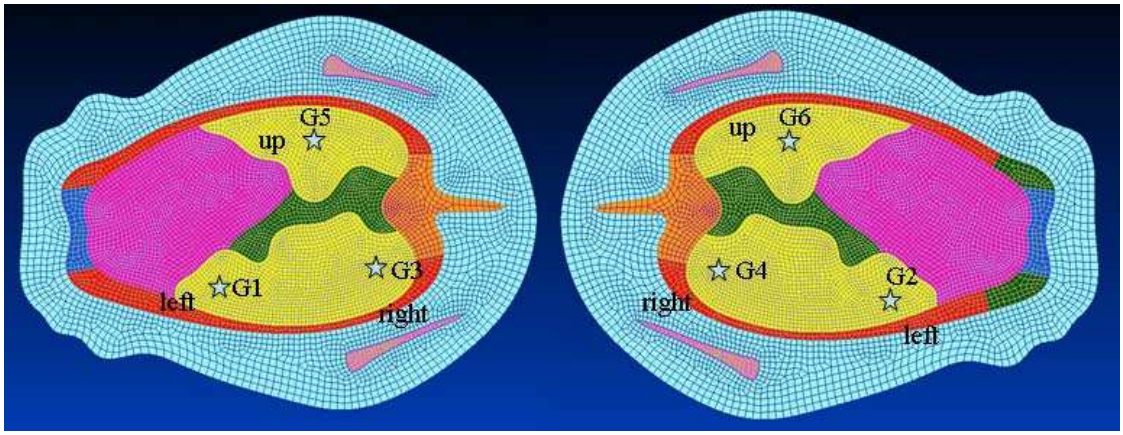

Figure 23: Gauge locations for body orientation inputs, sheep.

6.1 TH-T_2-P_{200} case

Figures 24 and 25 represent the blast injury that would results in the human and sheep lung for twelve different orientations. The distribution of injury based on the maximum peak pressures in the FE human and sheep lungs ranged from no injury, trace, slight, moderate, to severe according to Table 4. Figure 24 is for the lower layer of elements in the human model, where the rib cage is represented by intercostal muscle tissue. Figure 25 is the corresponding plots for the sheep model. Figure 26 shows a polar plot of the maximum human and sheep lung pressures as a function of orientation of the blast loading. From the TH-T_2-P_{200} figures, when the blast impacts a human torso in angle varying between 330 deg to 30 deg in the clockwise direction, the blast is predicted to induce significant lung injuries. In the sheep case, the TH-T_2-P_{200} blast is predicted to have negligible effects on the sheep lung irrespective of the orientation.

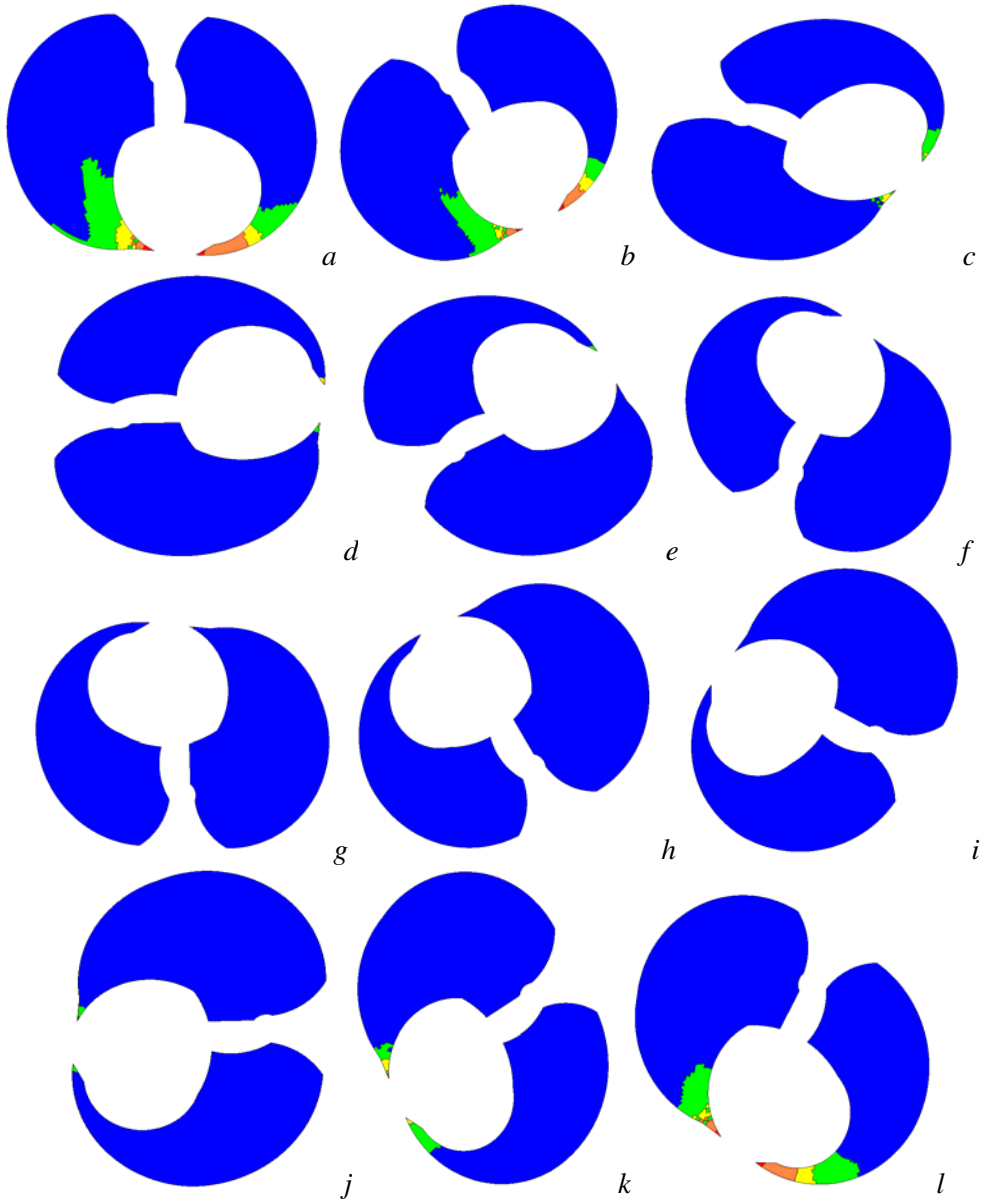

Figure 24: Maximum human lung overpressure for different orientations with respect to blast origin, TH-T_2-P_{200}, a= 0, b=30, c=60, d=90, e=120, f=150, g=180, h=210, i=240, j=270, k=300 and l=330 deg

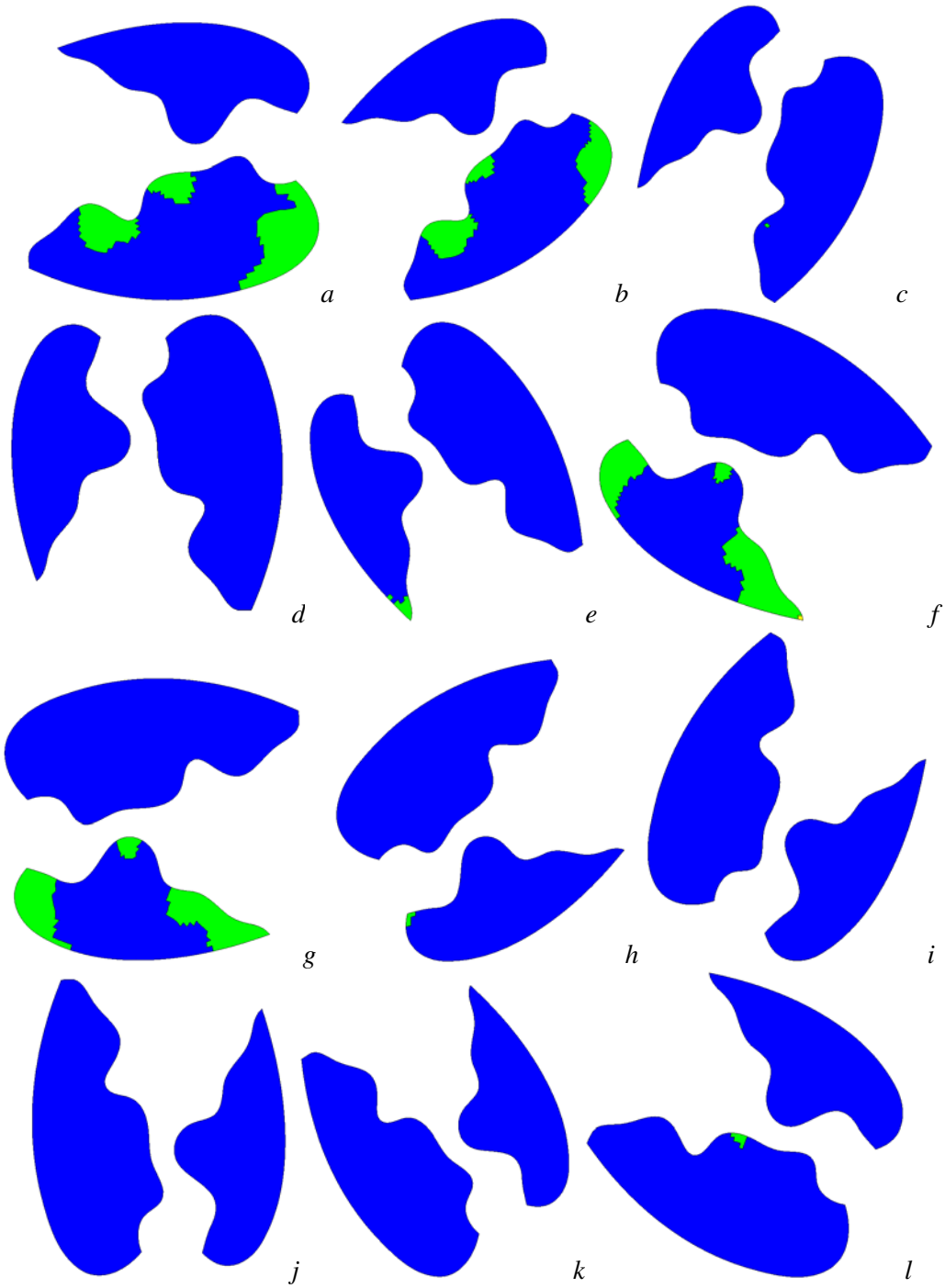

Figure 25: Maximum sheep lung overpressure for different orientations with respect to blast origin, TH-T_2-P_{200}, a= 0, b=30, c=60, d=90, e=120, f=150, g=180, h=210, i=240, j=270, k=300 and l=330 deg.

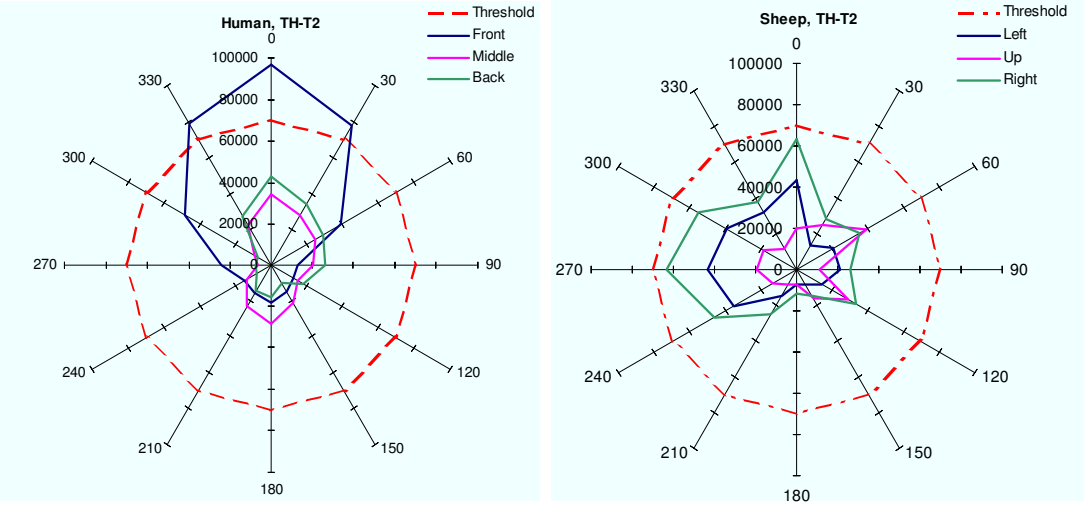

Figure 26: Maximum human and sheep lung overpressure for different orientations with respect to blast origin, TH-T_2-P_{200}

6.1.1 LD_1-T_2-P_{500} case

Figure 27 shows an interesting result obtained using the LD_1-T_2-P_{500} loading. The LD_1-T_2-P_{500} blast case induces only slight effects on the human lung when the torso is in the 90 deg to 270 deg positions (clockwise direction). In addition, the 0 deg (*a*) and 180 deg (*g*) cases have different distributions of the maximum lung overpressure. Based on the numerical results, blasts induce more injury in the 0 deg case than the 180 deg case. The same trend was observed with the 30 deg case and 210 deg case.

This tendency was not observed in the sheep case where only the specific orientations of 90 deg, 240 deg and 300 deg are predicted to induce only slight damage to the sheep lung (Figure 28). All other orientations are predicted to result in significant injury in at least one lung.

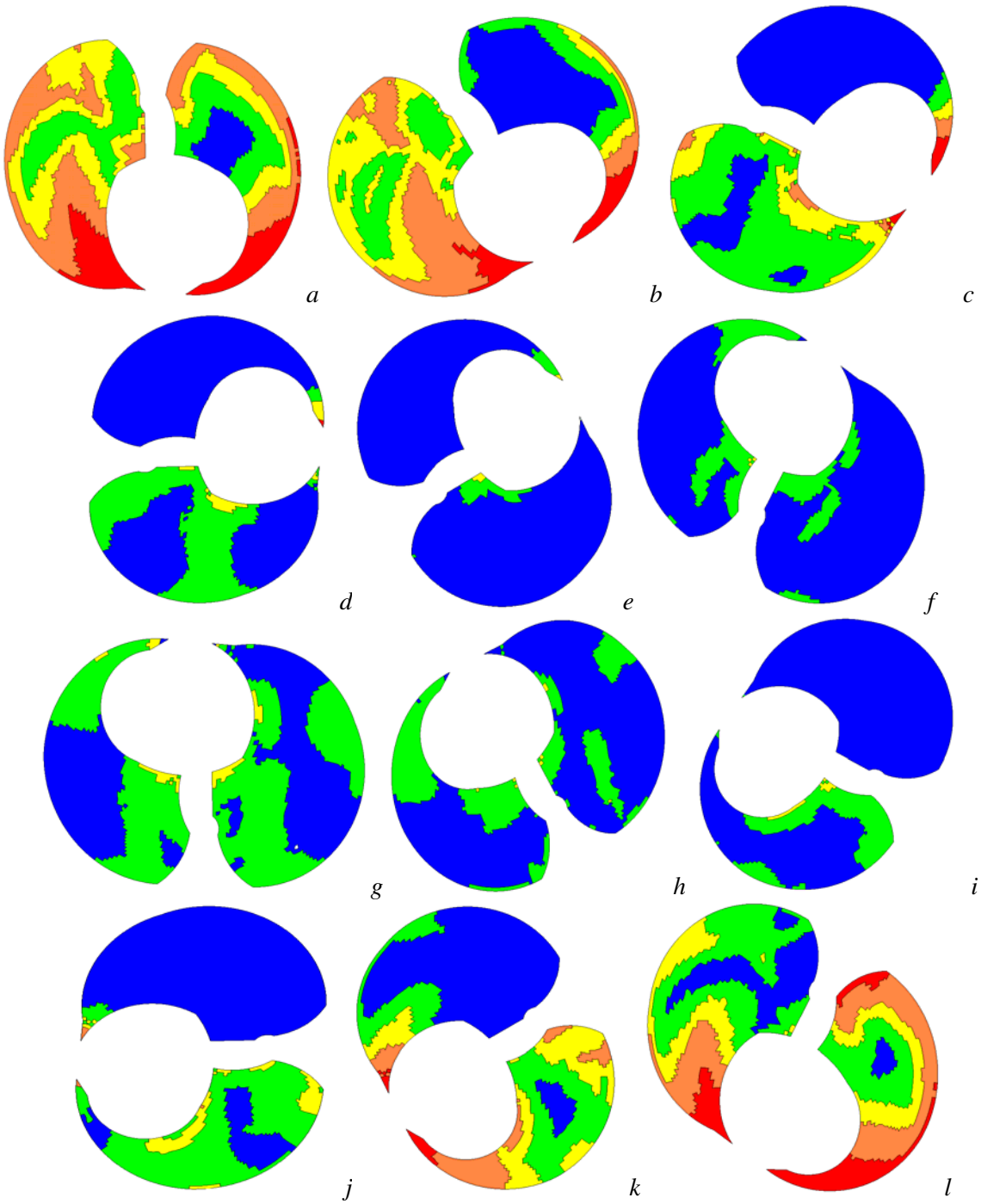

Figure 27: Maximum human lung overpressure for different orientations with respect to blast origin, LD_1-T_2-P_{500}, a= 0, b=30, c=60, d=90, e=120, f=150, g=180, h=210, i=240, j=270, k=300 and l=330 deg.

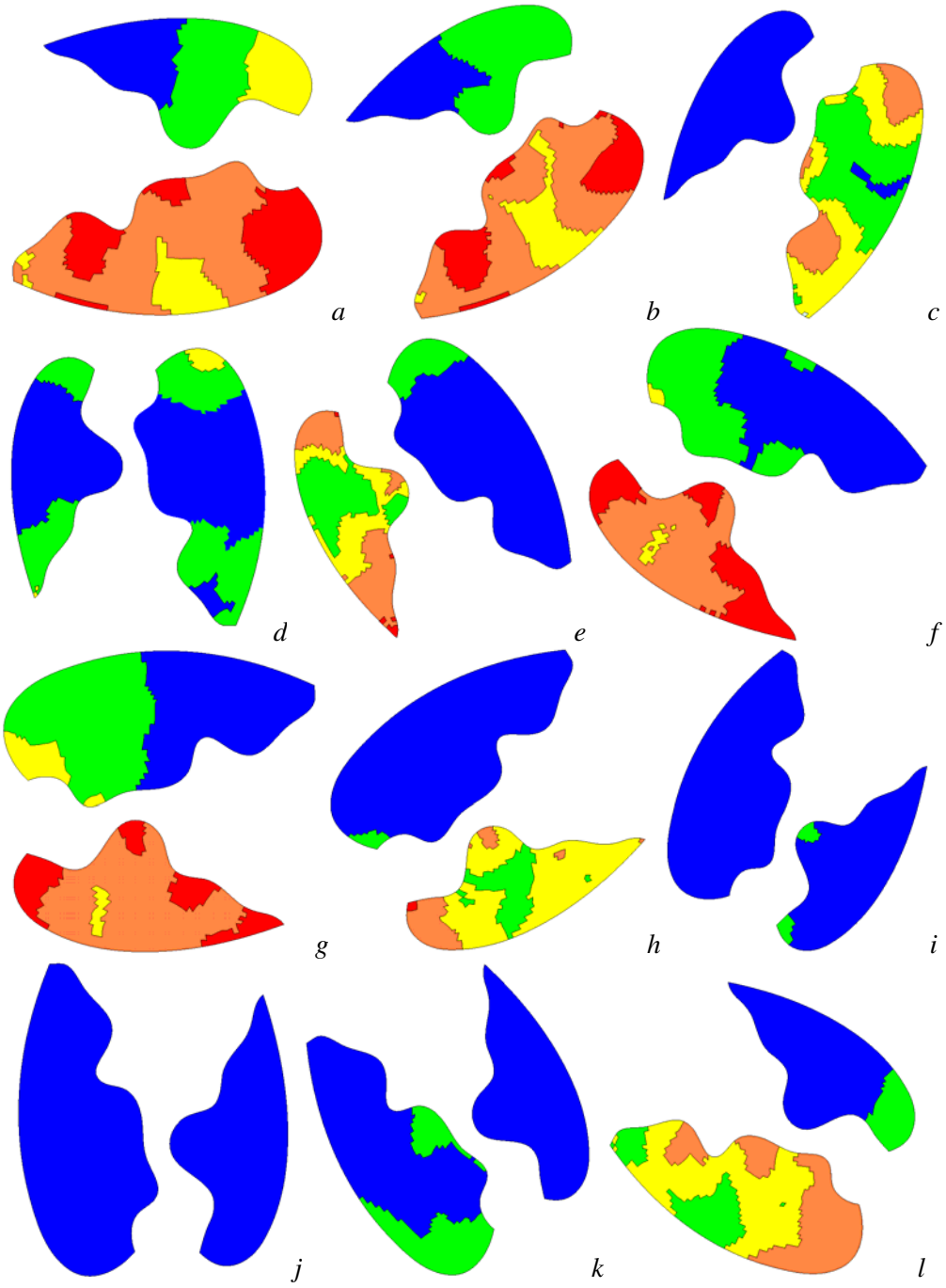

Figure 28: Maximum sheep lung overpressure for different orientations with respect to blast origin, LD_1-T_2-P_{500}, a= 0, b=30, c=60, d=90, e=120, f=150, g=180, h=210, i=240, j=270, k=300 and l=330 deg.

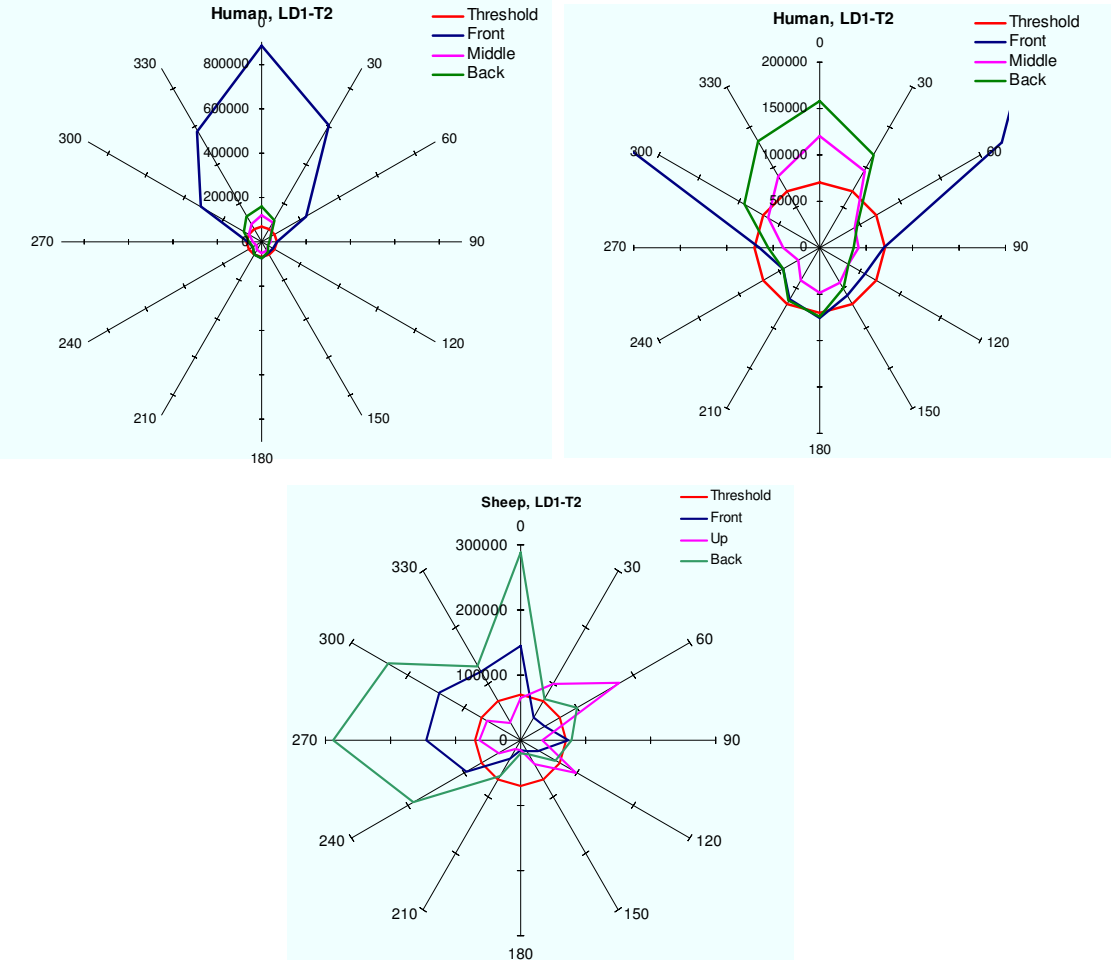

Figure 29: Maximum overpressure in human and sheep lungs for different orientation, LD_1-T_2-P_{500}

6.1.2 LD_{50}-T_2-P_{700} case

The same trend observed from the LD_1-T_2-P_{500} loading is also noticed when using the LD_{50}-T_2-P_{700} loading histories. The LD_{50}-T_2-P_{700} blast is predicted to have slight effects in the cases where the human torso is in the 120 deg to 240 deg positions (clockwise direction). If this reduced sensitivity to blast in these orientations can be proven in humans, it could be a significant driver when designing future protection against blasts. For example, the blast protection for the torso could cover the arc from 300 to 60 deg in the clockwise direction. In the sheep case, only the 240 deg and 270 deg cases induce slight blast injuries in the lungs with significant injuries being predicted in at least one lung in all other cases.

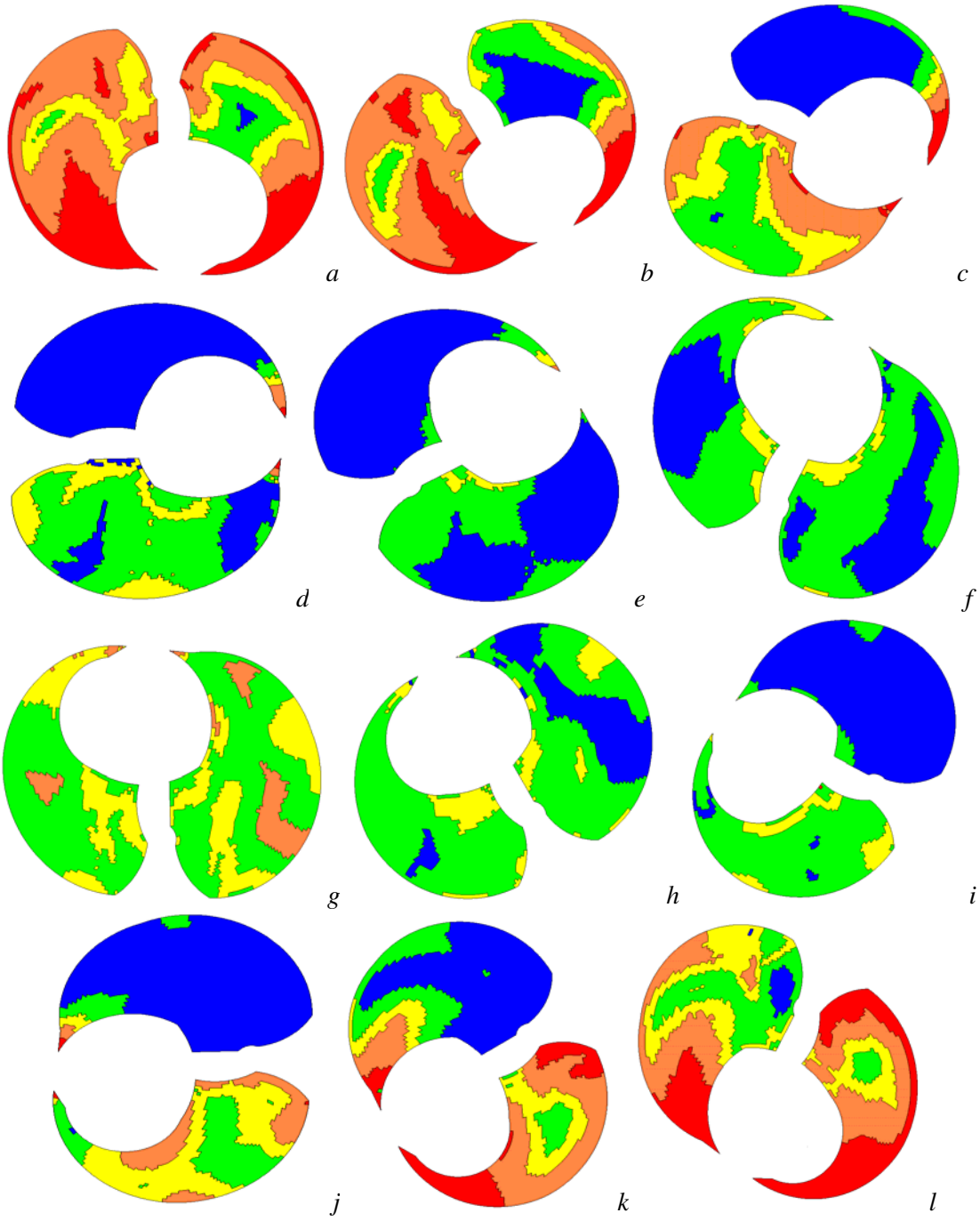

Figure 30: Maximum human lung overpressure for different orientations with respect to blast origin, LD_{50}-T_2-P_{700}, a= 0, b=30, c=60, d=90, e=120, f=150, g=180, h=210, i=240, j=270, k=300 and l=330 deg.

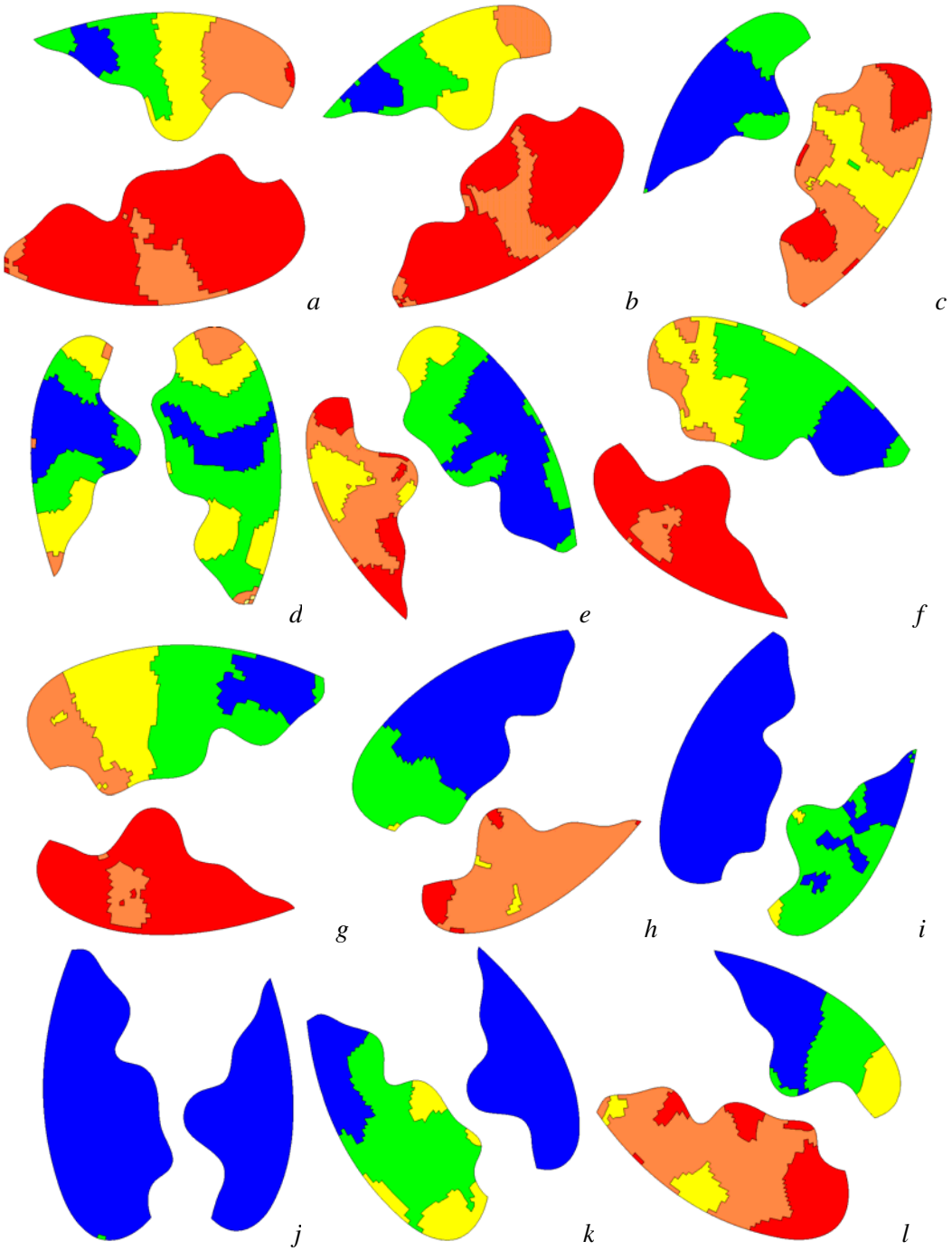

Figure 31: Maximum sheep lung overpressure for different orientations with respect to blast origin, LD_{50}-T_2-P_{700}, a= 0, b=30, c=60, d=90, e=120, f=150, g=180, h=210, i=240, j=270, k=300 and l=330 deg.

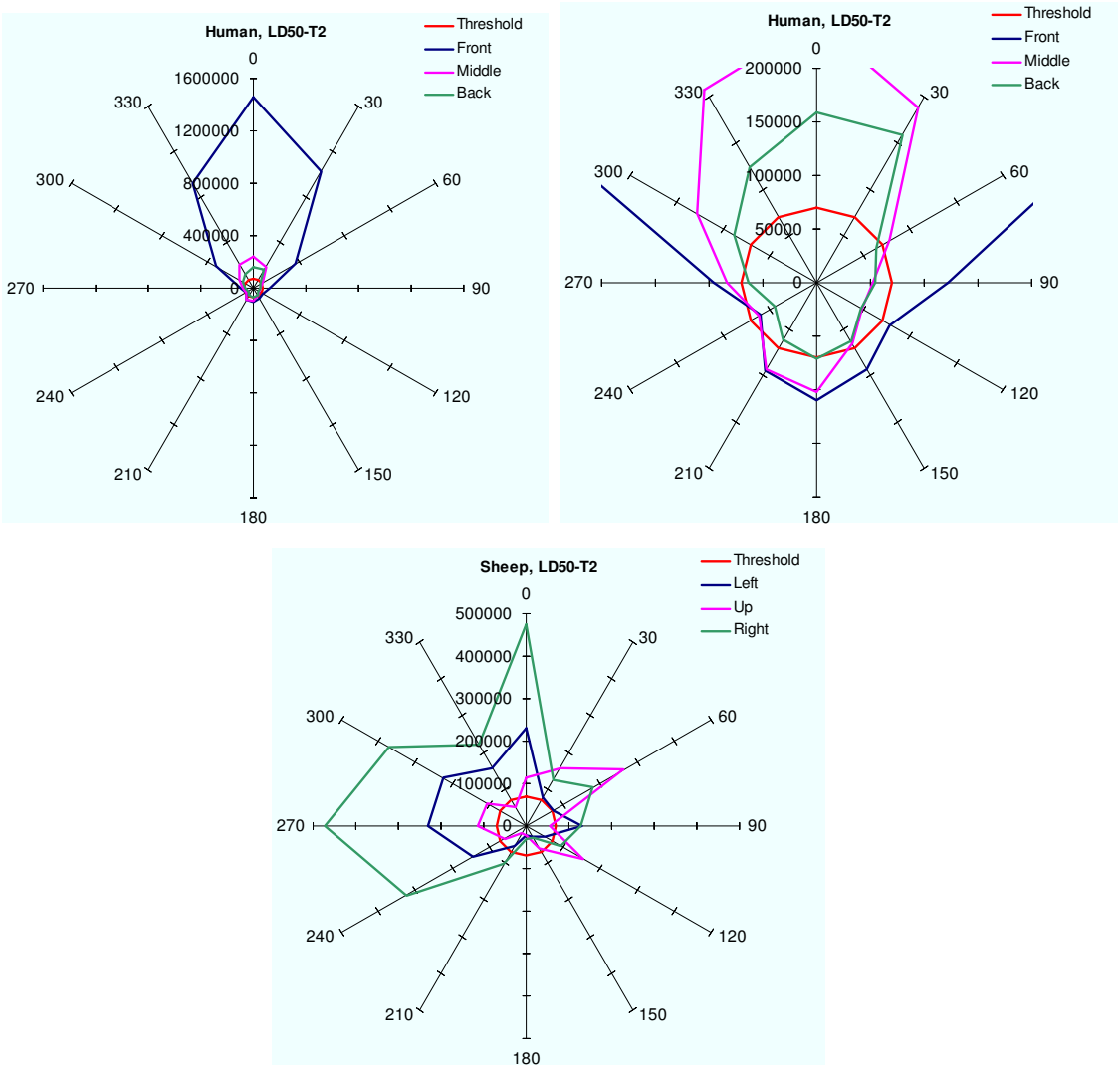

Figure 32: Maximum overpressure in human and sheep lungs for different orientations, LD_{50}-T_2-P_{700}

Table 8 summarizes the outcomes obtained from the numerous simulations run on the human and sheep torsos for different orientations to the blast wave. From this study, it is predicted that lung PBI (primary blast injury) may be reduced by focusing protection on the torso from -60 deg to +60 deg measured horizontally relative to the sternum.

Table 8: Summary of blast wave orientation, sheep and human lungs

	Human	**Sheep**
TH-T_2-P_{200}	None or trace injuries from 60 deg to 300 deg	No significant injuries in all orientation
LD_1-T_2-P_{500}	None or trace injuries from 90 deg to 270 deg	None or trace injuries from 240 deg to 300 deg
LD_{50}-T_2-P_{700}	Slight and severe injuries in all orientations	None or trace injuries from 240 deg to 270 deg

7 Complex blast

7.1 Loading condition

Three complex blast curves with known peaks and durations were used to simulate their effect on human and sheep lungs. These curves were recorded during experimental tests on the DRDC-MABIL mannequin placed at 2 m, 2.5 m and 3.5 m from a 5 kg C4 explosive charge and are labelled respectively as CW_1, CW_2 and CW_3 in Figure 33. Figure 33 shows a comparison between the measured blast overpressure histories and the loading replicated in the numerical model. Again, the excellent fit curves are the result of considerable curve fitting efforts [Ref. 12].

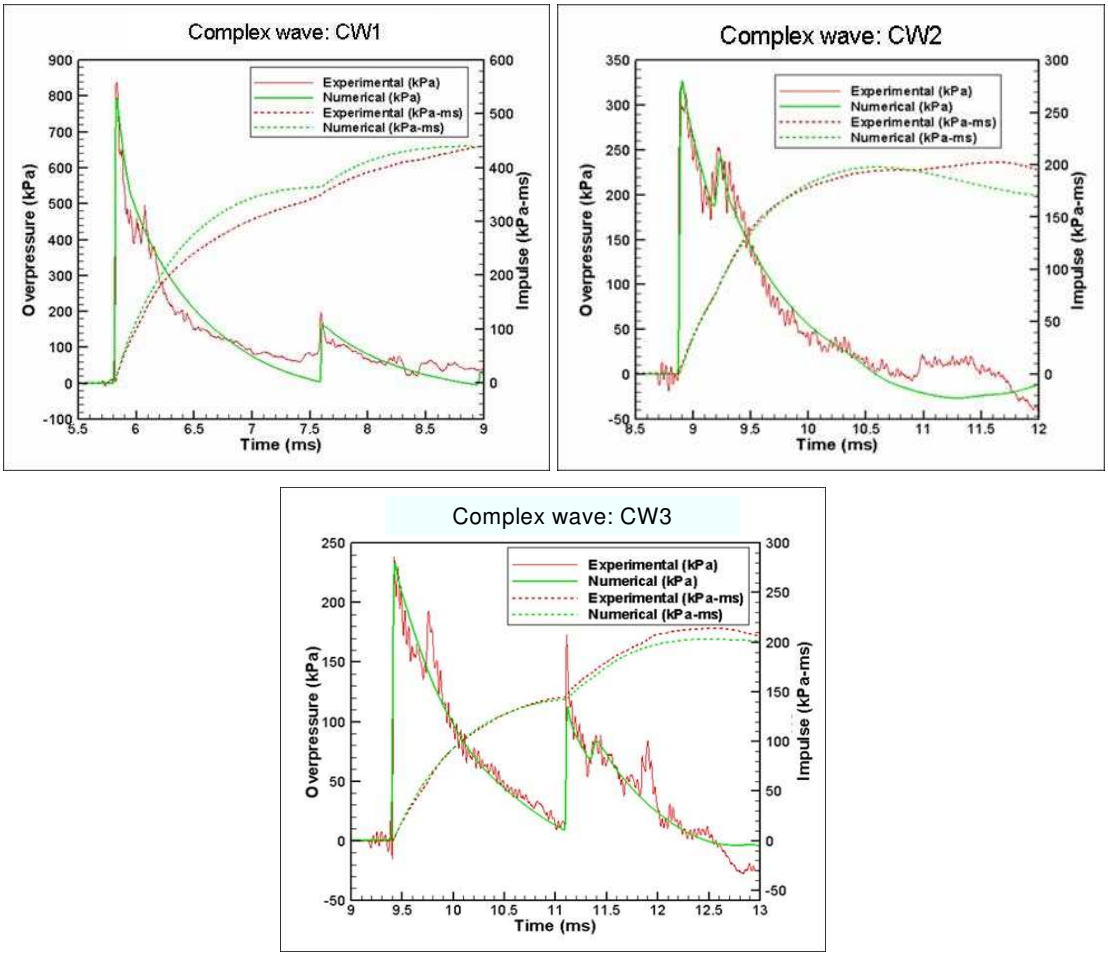

Figure 33: Complex blast curves based on experimental traces.

7.2 Complex blast assumption

The 1.5 m burst height used in the experimental trial results in the shock wave being reflected from the ground, which in turn creates a complex blast wave with two peaks at the location of the mannequins and pressure gauges. Even if these experimental blasts cannot be considered to be ideal Friedlander waves it is possible to use the peak overpressure and an estimate of the positive phase duration to obtain a rough estimate of the expected lethality using the Bowen curves [Ref. 4]. This procedure is widely used to allow the application of empirical injury models with non-ideal experimental data, although it is the subject of some debate. Based on this approximation, the time-pressure histories from the CW_1, CW_2 and CW_3 curves correspond approximately to LD_{99}-T_4-P_{800}, TH-T_2-P_{330} and TH-T_4-P_{240}. Using this approximation, the three complex waves can be located on the Bowen chart and they are given in Figure 34.

From Figure 34, CW_2 and CW_3 are approximately on the same Bowen iso-injury curve. Consequently, they would be predicted to cause the same level of injury. The CW_2 and CW_3 blast waves have the same total impulse, which is approximately 200 kPa·ms but different durations (2 ms and 3.5 ms respectively) and different ratios between the first and second peak overpressures. In the case of CW_2, the ratio between the first and second peak overpressure is 1.32 whereas in CW_3, the ratio is 2.18. The CW_1 and CW_3 have the same blast wave duration (4 ms) but the CW_1 blast corresponds to approximately twice the total impulse of the CW_3 blast wave. As a result, these three loading histories represent an interesting case study to try to isolate the influence of characteristics of complex blast wave (albeit relatively simple complex waves) on the lung injury induced.

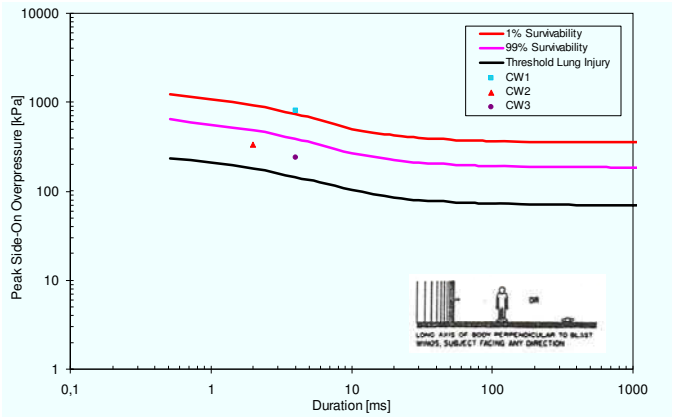

Figure 34: CW_1, CW_2 and CW_3 on the revised Bowen curves by Richmond.

7.3 Results

The maximum human and sheep lung damage for the three complex blasts are shown in Figures 35 to 38. The lung damage was ranked from *none* to *severe* using Table 4. Examining the distribution of the peak pressures shows that injury to the human and sheep lungs is greater in the CW_2 case than for the CW_3 loading, even though the two blasts have the same total impulse and are located on the same modified Bowen iso-injury curves. The predicted injury to the lung may be explained by the blast wave overpressure of CW_2 being higher than the blast wave overpressure of CW_3 or by the difference in the ratio between the first and the second peak overpressure in both blasts. In the case of CW_2, this ratio is 1.32 whereas in CW_3, it is 2.18. The CW_1 and CW_3 loading histories have the same duration (4 ms) but different peak overpressure. Damage to the lung is thought to be more severe in the CW_1 blast wave due to the higher peak overpressure.

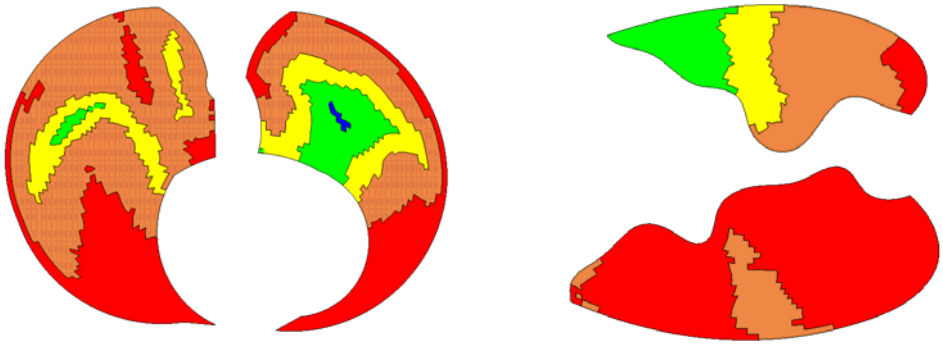

Figure 35: Comparison of blast damage to human and sheep lungs resulting from exposure to complex CW_1 blast loading history.

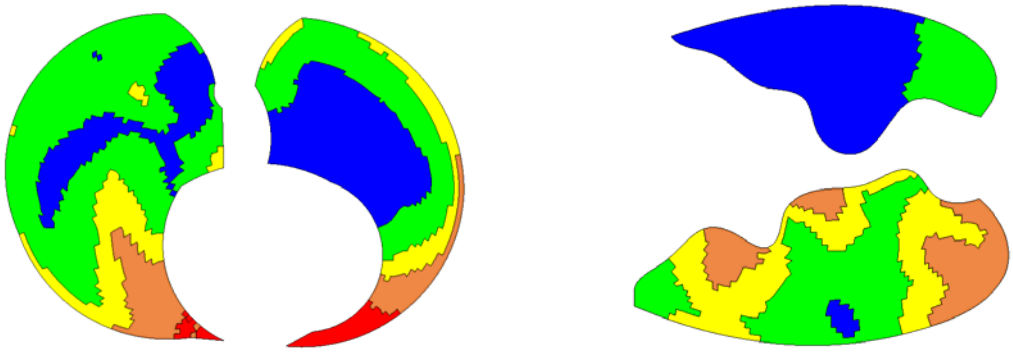

Figure 36: Comparison of blast damage to human and sheep lungs resulting from exposure to CW_2 blast loading history.

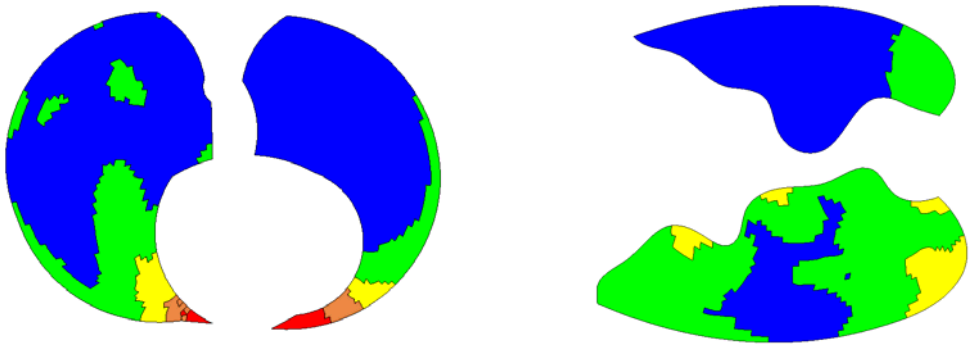

Figure 37: Comparison of blast damage to human and sheep lungs resulting from exposure to CW_3 blast loading history.

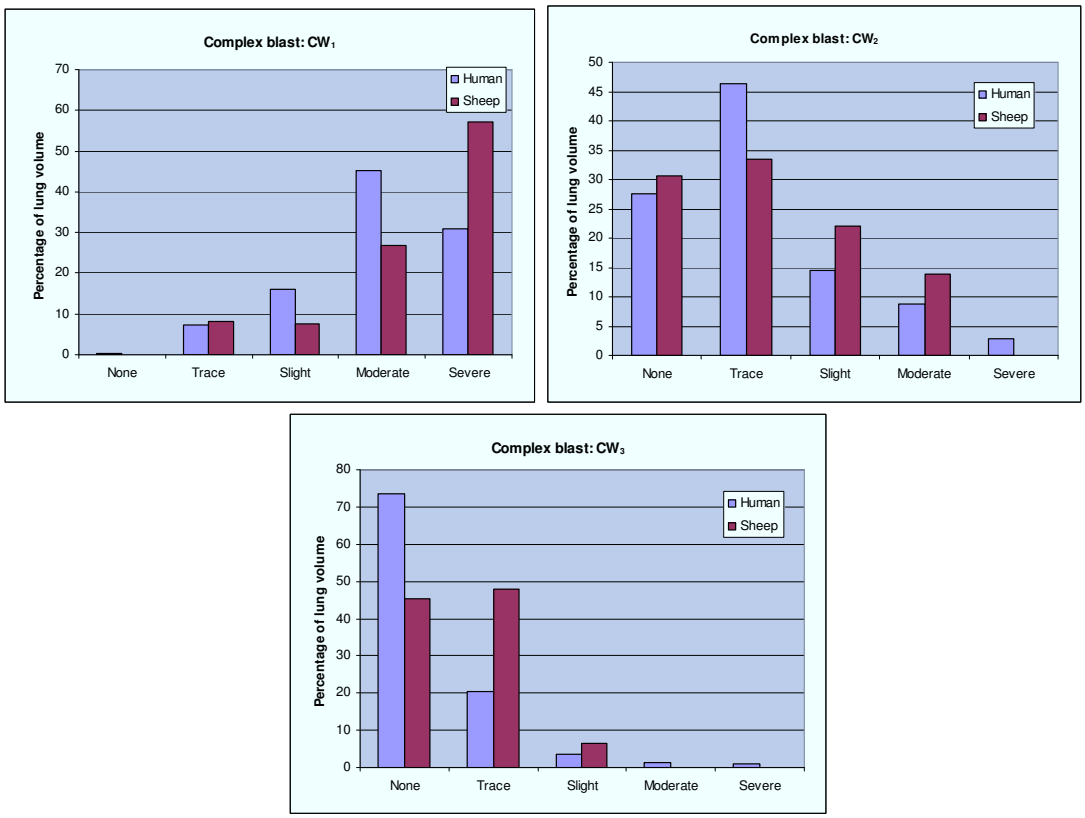

Figure 38: Percentage of human and sheep lung damage for complex blasts CW_1, CW_2 and CW_3

8 Conclusion

Quasi-two-dimensional FE models of a human and sheep thorax were developed using the non-linear arbitrary Lagrangian-Eulerian formulation in LS-DYNA. The FE models were applied to studies of free field and complex blast loading as well as a study of the effect of body orientation to the blast wave. The numerical results were then validated for lung primary blast injury (PBI) with the limited data available in the open literature including the Bowen curves.

Sheep may be used as a substitute during experimental blast tests. However, numerical results show that humans have higher tolerance to blast than sheep at short blast wave durations. Also, lung PBI in sheep is more sensitive to the blast wave duration. In fact, the longer overpressure durations studied here (e.g. 5 ms) are predicted to induce higher pressures in the sheep lung than in the human lung. In all 5 ms duration overpressure cases studied, pressures in the sheep lung were approximately twice those in the human lung.

A parametric study was performed to investigate the effect of blast wave orientation on the human and sheep lungs. From this study, it is predicted that the greatest reduction in lung PBI may be come from focusing protection on the torso from -60 deg to +60 deg measured horizontally relative to the sternum.

An assumption was made to approximate complex blasts with Friedlander waves. Two complex blasts (CW_2 and CW_3) were approximated by the TH-T_2-P_{330} and TH-T_4-P_{240} curves respectively and were located at the threshold level of the Bowen curves revised by Richmond. Numerical results showed that the maximum lung overpressure in human and sheep lungs for the CW_2 and CW_3 complex blasts exceeded the threshold level (70 kPa). This assumption is therefore not correct raising questions as to the applicability of the Bowen curves to estimating lethality from complex blasts. Further study is warranted.

Further enhancements can be made to the torso model. First, the model itself could be refined by allowing contact between the lung components. Second, other two-dimensional slices taken at different levels in the human and sheep thoraces, or indeed a three-dimensional human and sheep torso model, should be modelled since only injuries between the fifth and sixth vertebrae level were studied and generalized as predictors of overall lung injury. Third, the model developed in the present study does not allow wave propagation on the vertical axis (principle axis of the body). It would also be worthwhile to study the curves by Bass et al. to see if there is better agreement between numerical and analytical results. Also, a Hopkinson sheep-mass-scaling in relation to human have to be done. This study may explain why humans are predicted to have higher tolerance to blast than sheep. Finally, the next step of this study is to investigate different thoracic blast protection concepts.

References

[1] http://www.emedicine.com. February, 2007.

[2] Salisbury, S., Greer, A. and Duane, C., 2004, "*Numerical modelling of blast injuries*'', University of Waterloo, Contractor report, W7701-024463/001/QCA.

[3] Hallquist, J., 2006, "LS-DYNA User's Manual ver. 970", Livermore Software Technology Corporation, Livermore, California.

[4] Bowen, I.G., Fletcher, E.R., Richmond, D.R., Hirsch, F.G. and White, C.S., 1968, "*Biophysical Mechanisms and scaling procedures applicable in assessing responses of the thorax energized by air-blast overpressures or by nonpenetrating missiles*", Ann. N.Y. Acad. Sci. 152, pp. 122-146.

[5] Richmond, D., Private communication, 2003.

[6] Bass R.C., Rafaels K. and Salzar R., *Pulmonary injury risk assessment for short-duration blasts*, Personal Armor Systems Symposium 2006, Leeds, UK, 2006, p233-246

[7] O'Brien, W.D. and Zachary, J.F., 1996, "*Rabbit and pig lung damage comparison from exposure to continuous wave 30-kHz ultrasound*", Ultrasound in Med. And Biol. Vol. 22, No. 3.

[8] Cooper, G., Townend, D, Cater, S. and Pearce, B., 1991, "*The role of stress waves in thoracic visceral injury from blast loading: modification of stress transmission by foams and high-density materials*", Journal of Biomechanics Vol. 24, pp. 273-285.

[9] Stuhmiller, J., Chuong, C., Phillips, Y. and Dodd, K., 1988, "*Computer modelling of thoracic response to blast*", The Journal of Trauma, Vol. 28, No. 1 Supplement.

[10] http://www.nlm.nih.gov February, 2007.

[11] Davies, A.S., Garden, K.L., Young, M.J. and Reid, C.S.W., 1987, "*An atlas of X-ray tomographical anatomy of the sheep*'', Science Information Publishing Centre, Wellington, New Zealand.

[12] Dunbar, T. and Donahue, L., *Generation of load curves for LS-Dyna torso model*, Martec Limited, Contractor report for DRDC Valcartier. CR 2006-597.

Annex A Human lung overpressure

Polar plots of the maximum overpressure in human lungs at different virtual gauges. The location of these gauges is identified in section 6 of the present study.

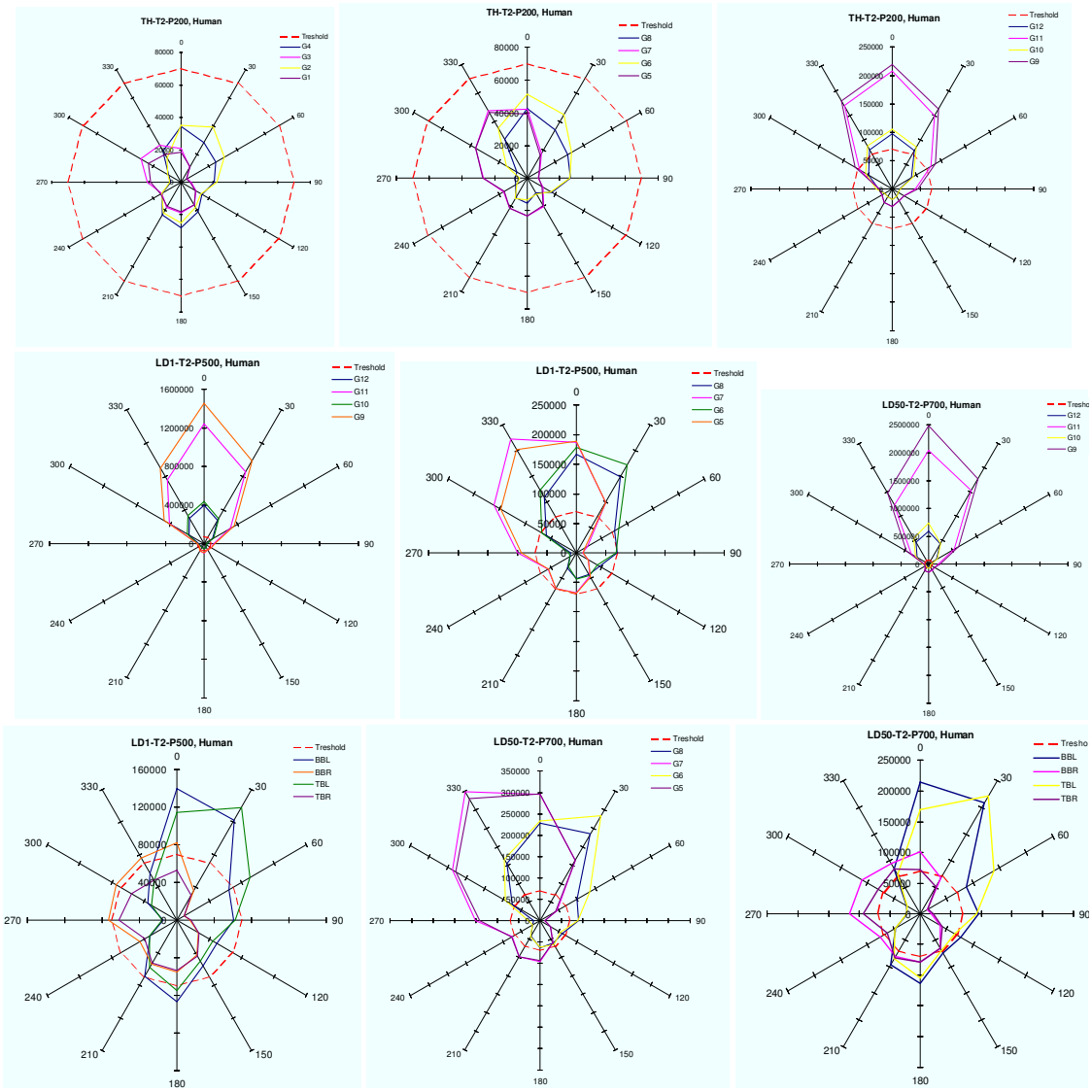

Figure A-1: Maximum human lung overpressure for different orientations

This page intentionally left blank.

List of symbols/abbreviations/acronyms/initialisms

ALE	Arbitrary Lagrangian-Eulerian method
CW_1	Complex wave 1
CW_2	Complex wave 2
CW_3	Complex wave 3
DRDC	Defence Research & Development Canada
FE	Finite element
GI	Gastrointestinal
IED	Improvised explosive device
LD_1	1% probability of lethal dose
LD_{50}	50% probability of lethal dose
LD_{99}	99% probability of lethal dose
PBI	Primary blast injuries
TH	Threshold

This page intentionally left blank.